NAVAL POSTGRADUATE SCHOOL

MONTEREY, CALIFORNIA

THESIS

SIMULTANEOUS DUAL LASER STABILIZATION FOR STRONTIUM ATOM INTERFEROMETRY

by

Matthew D. Spakowski

September 2022

Thesis Advisor: Frank A. Narducci
Second Reader: Gamani Karunasiri

THIS PAGE INTENTIONALLY LEFT BLANK

REPORT DOCUMENTATION PAGE			*Form Approved OMB No. 0704-0188*

1. AGENCY USE ONLY *(Leave blank)*	**2. REPORT DATE** September 2022	**3. REPORT TYPE AND DATES COVERED** Master's thesis

4. TITLE AND SUBTITLE
SIMULTANEOUS DUAL LASER STABILIZATION FOR STRONTIUM ATOM INTERFEROMETRY

5. FUNDING NUMBERS
RPPD6; RPP6N

6. AUTHOR(S) Matthew D. Spakowski

7. PERFORMING ORGANIZATION NAME(S) AND ADDRESS(ES)
Naval Postgraduate School
Monterey, CA 93943-5000

8. PERFORMING ORGANIZATION REPORT NUMBER

9. SPONSORING / MONITORING AGENCY NAME(S) AND ADDRESS(ES)
Army Research Office, Research Triangle, NC, 277703

10. SPONSORING / MONITORING AGENCY REPORT NUMBER

11. SUPPLEMENTARY NOTES The views expressed in this thesis are those of the author and do not reflect the official policy or position of the Department of Defense or the U.S. Government.

12a. DISTRIBUTION / AVAILABILITY STATEMENT
Approved for public release. Distribution is unlimited.

12b. DISTRIBUTION CODE
A

13. ABSTRACT (maximum 200 words)

The use of strontium in an atom interferometer presents the opportunity to perform detailed measurements of gravitational fields, rotation rates, and clock transitions as well as other natural phenomena. Strontium can be particularly effective in atom interferometry experiments for two reasons. The first is that the intrinsic magnetic properties of strontium result in less sensitivity of the transition frequencies to magnetic noise, allowing for better measurements. Second, strontium atoms can be cooled to a lower temperature just through ordinary Doppler cooling than other atoms typically used in interferometry (e.g., rubidium). A lower temperature means less initial kinetic energy and hence lower spatial dispersion over the course of an experiment. A magneto-optical trap consisting of two primary cooling lasers and two repump lasers cools and confines strontium atoms for use in the interferometer. This thesis focuses on the repump lasers and includes the design and performance of the optical system that frequency stabilizes each laser. The system demonstrated the ability to simultaneously frequency lock the two repump lasers to the degree necessary to form a strontium magneto-optical trap.

14. SUBJECT TERMS atom interferometry, laser cooling, strontium, magneto-optical trap	**15. NUMBER OF PAGES** 97
	16. PRICE CODE

17. SECURITY CLASSIFICATION OF REPORT	**18. SECURITY CLASSIFICATION OF THIS PAGE**	**19. SECURITY CLASSIFICATION OF ABSTRACT**	**20. LIMITATION OF ABSTRACT**
Unclassified	Unclassified	Unclassified	UU

NSN 7540-01-280-5500

Standard Form 298 (Rev. 2-89)
Prescribed by ANSI Std. 239-18

THIS PAGE INTENTIONALLY LEFT BLANK

Approved for public release. Distribution is unlimited.

SIMULTANEOUS DUAL LASER STABILIZATION FOR STRONTIUM ATOM INTERFEROMETRY

Matthew D. Spakowski
Lieutenant Commander, United States Navy
BS, United States Air Force Academy, 2007
MEM, Old Dominion University, 2015

Submitted in partial fulfillment of the
requirements for the degree of

MASTER OF SCIENCE IN PHYSICS

from the

NAVAL POSTGRADUATE SCHOOL
September 2022

Approved by: Frank A. Narducci
Advisor

Gamani Karunasiri
Second Reader

Frank A. Narducci
Chair, Department of Physics

THIS PAGE INTENTIONALLY LEFT BLANK

ABSTRACT

The use of strontium in an atom interferometer presents the opportunity to perform detailed measurements of gravitational fields, rotation rates, and clock transitions as well as other natural phenomena. Strontium can be particularly effective in atom interferometry experiments for two reasons. The first is that the intrinsic magnetic properties of strontium result in less sensitivity of the transition frequencies to magnetic noise, allowing for better measurements. Second, strontium atoms can be cooled to a lower temperature just through ordinary Doppler cooling than other atoms typically used in interferometry (e.g., rubidium). A lower temperature means less initial kinetic energy and hence lower spatial dispersion over the course of an experiment. A magneto-optical trap consisting of two primary cooling lasers and two repump lasers cools and confines strontium atoms for use in the interferometer. This thesis focuses on the repump lasers and includes the design and performance of the optical system that frequency stabilizes each laser. The system demonstrated the ability to simultaneously frequency lock the two repump lasers to the degree necessary to form a strontium magneto-optical trap.

THIS PAGE INTENTIONALLY LEFT BLANK

Table of Contents

List of Figures

List of Tables

THIS PAGE INTENTIONALLY LEFT BLANK

List of Acronyms and Abbreviations

AOM	acousto-optic modulator
ADEV	Allan deviation
FWHM	full width at half maximum
HCL	hollow cathode lamp
HVAC	heating ventilation and air conditioning
MOT	magneto-optical trap
NIST	National Institute of Standards and Technology
NPS	Naval Postgraduate School
PBS	polarizing beam splitter
PID	proportional, integral, differential

THIS PAGE INTENTIONALLY LEFT BLANK

Executive Summary

Atom interferometry experiments at the Naval Postgraduate School to date used rubidium atoms. The Quantum Sensing Lab team is in the initial stages of constructing a 30 meter atomic tower that will use strontium atoms because the properties of strontium enable more precise measurements. Strontium, as a Group II element has paired electrons in its valence shell giving the bosonic isotopes no net angular momentum. This configuration limits the influence of magnetic fields on the transition frequencies which leads to more accurate measurements. Strontium also has two transitions that can be used for cooling. The first broad transition can quickly capture a large amount of atoms, and the second narrower transition can cool the atoms to a much lower temperature through normal Doppler cooling. At a lower temperature the atoms disperse less again leading to more accurate measurements. Therefore, strontium is the choice to make precision measurements of parameters such as gravity, rotation rates, and magnetic fields in the 30 meter tower.

To maximize the number of atoms available for study, the magneto-optical trap for strontium uses two repump lasers. These lasers increase the amount of time that atoms are available for cooling by preventing them from staying in long lived excited states. In strontium these lasers drive excited state transitions, specifically at 707 nm and 679 nm wavelengths.

This thesis presents the optical system used to simultaneously frequency stabilize the two repump lasers for use in a strontium magneto-optical trap. Using the absorption characteristics of light passing through a sample of strontium atoms, I generated a feedback signal to the controllers for each of the two repump lasers. The system performed better for the 707 nm laser than the 679 nm laser, but this was expected since the 707 nm transition is a stronger transition. The locking system I developed successfully held a frequency lock over an extended period of time, reduced long term frequency drifts, and limited the frequency spread of the lasers. For the 707 nm laser the standard deviation of the observed laser frequency was significantly less than the natural linewidth of the transition, while for the 679 nm laser the standard deviation was on the order of the natural linewidth of the transition. Overall, the locking system effectively simultaneously frequency stabilized both repump lasers to the degree necessary to form a strontium magneto-optical trap.

Tuned and stable repump lasers are vital because they maximize the number of atoms that can be trapped and used for atom interferometry. Therefore the system I developed is an integral component of the atom interferometry setup for making precision measurements.

THIS PAGE INTENTIONALLY LEFT BLANK

Acknowledgments

I would first like to thank my family for all of their support and understanding. Next I would like to thank Professor Frank Narducci and Dr. Jeffrey Lee for all their time, insight, and patience to explain and re-explain the physics I had the privilege to learn along the way.

THIS PAGE INTENTIONALLY LEFT BLANK

CHAPTER 1:
Introduction

Precision measurements of the fundamental constants of nature such as the universal gravitational constant, G, or the fine structure constant, α, are of great academic interest. These measurements reveal fundamental truths about the structure of the universe as well as drive the development of more capable techniques and methods to achieve greater and greater precision. Beginning in the early 1990s, the scientific community used atom interferometry to make precision measurements of fundamental constants [1], [2]. This technique leverages the dual wave and particle nature of atoms by propagating them in a superposition of states, allowing them to accumulate phase based on their interaction with the forces of nature, and observing the results.

Atom interferometers can also be used to measure practical parameters such as local gravitational acceleration [1], [3], magnetic field gradients [4], and rotation rates [5]. These types of measurements have important potential military applications since they can be used to develop highly sensitive sensors. For example, highly accurate and precise measurements of rotation can be used to make gyroscopes for inertial navigation. Additionally the ability to detect minute changes in a magnetic field can be useful for locating submarines. One significant challenge is making the system that performs atom interferometry functionally capable of operating in field conditions. Due to the scale, precision, and technical sophistication necessary for these techniques, atom interferometry is predominantly done in the laboratory. Transitioning these systems to the field requires significant and investment as well as definitive demonstration of their utility.

Most previous atom interferometry experiments, used sodium, rubidium, or cesium, as their object of study. Atom interferometry experiments to date at Naval Postgraduate School (NPS) used rubidium atoms. These species of atoms are all Group I elements with one unpaired valence electron. The method of cooling and trapping them for use in experiments involves one cooling laser and one repump laser. Also, the target transition for both the cooling and repump laser involves a ground state electron. In recent years strontium, a Group II element with two valence electrons, has become an interesting object of study. Due to the different spectroscopy and magnetic properties of strontium these atoms can be cooled further with normal Doppler cooling and they are less susceptible to stray magnetic fields. However, the different structure of strontium requires the development of

a much different scheme and strategy for trapping the atoms for use in atom interferometry experiments. This includes implementing multiple cooling lasers as well as working with excited state transitions for the repump lasers.

This thesis presents some of the initial work required for the development and construction of the planned 30 meter tower for strontium atom interferometry experiments at NPS. Specifically, my thesis focused on the two repump lasers required to form and optimize a magneto-optical trap (MOT) for strontium atoms. These lasers at 707 nm and 679 nm target excited state transitions of strontium and ensure strontium atoms do not spend excessive time in long-lived states that are not available for cooling. They accomplish this goal by exciting a strontium atom out of long-lived state where they can more quickly decay back to the ground state that is the target of the main cooling laser. In order to be effective, the frequency of these repump lasers must be stable and accurately tuned. A general rule is that the frequency spread of the laser over the time period of interest should be much less than the natural linewidth of the target transition. I further develop the criteria for determining the effectiveness of laser stabilization in Appendix B. In terms of accuracy, the tuning system requires a reference standard to ensure the laser frequency is properly set to drive the target transition. The best standard to use is the atoms themselves since the transition frequencies are properties of nature.

For my thesis, I developed and implemented an optical system to simultaneously stabilize and control the frequency of both repump lasers to optimize the effectiveness of a strontium MOT. In Chapter 2, I examine the theoretical basis underlying the key aspects of atom interferometry with strontium. Next, in Chapter 3, I present the optical system I developed to simultaneously frequency stabilize both repump lasers for use in strontium atom interferometry and its characteristics. In Chapter 4, I review the results and performance of the frequency stabilization system and outline future work required. Overall this thesis demonstrated an important capability for performing precision measurements using atom interferometry.

CHAPTER 2:
Background and Theory

In this chapter, I present the necessary background information for my thesis. I start with the theory and mechanism of atom interferometry, and then provide an estimate of how sensitive an atom interferometer can be for measuring physical parameters such as gravity. Next I take a building block approach and present the theory and operation of the systems needed to perform atom interferometry, including laser cooling of atoms and a description of a MOT. Afterwards I justify the use of strontium in the 30 meter tower experiments. To date, atom interferometry experiments at NPS used rubidium, whose electron configuration allows the use of Raman pulses which transfer atoms between different hyperfine ground states. Strontium's electron configuration has only one ground state so Raman pulses are not possible. Therefore, in the final section, I describe Bragg transitions, which given the properties of strontium, are essential to future atom interferometry experiments at NPS.

2.1 Atom Interferometers

The specific scheme and setup of an atom interferometry experiment depends on the phenomena to be studied. For the necessary background for this thesis, I consider an atom interferometer designed to measure gravity. In this type of atom interferometer a pulse of laser light puts the atom into a superposition of states. I discuss the exact mechanism of putting the atom in this superposition of states using Bragg transitions later in Section 2.4, but for now it means that after the pulse, the atom is in a superposition of having received a momentum kick by absorbing a photon and not having received a momentum kick. It is important to recognize the distinction between the electronic and momentum states of the atom. Ground or excited electronic states refer to whether or not all electrons in the atom occupy the lowest available orbital. Ground or excited momentum states refer to whether the atom has additional momentum from its interaction with a light pulse.

There are typically two types of pulses used in the interferometer. It should be stressed that, although the pulses are applied to a collection of atoms in an atom cloud, the effect is a single atom effect. The first pulse is called a $\pi/2$ pulse because it acts on the atoms such that it places half of the atomic population that may be in the ground state into the excited state and half that may be in the excited state into the ground state, resulting in a coherent superposition of ground and excited state [4]. The second type of pulse, called the π pulse,

places all of the population originally in the ground state into the excited state and all of the population originally in the excited state into the ground state [4].

The sequence of pulses depends on the objective of the experiment, but in this example, I consider the $\pi/2 - \pi - \pi/2$ pulse sequence depicted in Figure 2.1 and also described in [4]. As already mentioned, the first $\pi/2$ pulse puts each atom into a superposition of momentum states. If the atom starts in the ground state, then it needs not absorb momentum to stay in the ground state. To be promoted to the excited state, the atom needs to absorb momentum. Thus, the $\pi/2$ pulse creates a superposition of states with and without a momentum kick and the two parts of the atomic wavefunction start to separate. This effect is analogous to a beam splitter in an optical interferometer. Next, the π pulse flips the momentum state to begin to bring the two states back together, similar to a mirror in an optical interferometer. The final $\pi/2$ pulse closes the interferometer allowing meaningful measurements of the phase difference between the two paths and hence determining how gravity affected the amount of phase each path accumulated. This scheme, illustrated in Figure 2.1, sends each atom in a superposition of two different paths. At the end of the sequence, the number of atoms in an excited momentum state is proportional to the cosine of the difference in phase accumulated along each path. The interference is always between an atom and itself as it crosses the interferometer along different trajectories.

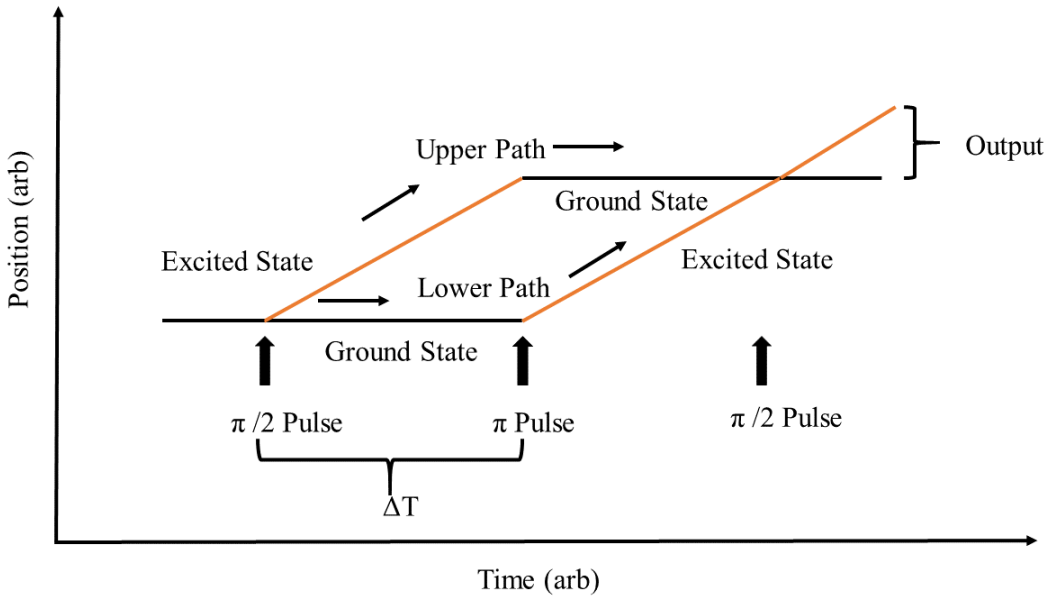

Figure 2.1. Schematic of an atom interferometer. Adapted from [4].

To calculate the phase difference between the upper and lower path of the interferometer I start with determining how much phase each path accumulates due to the classical action. This calculation is shown in Appendix A.1. As seen in the Appendix, as long as the time interval between the initial $\pi/2$ and π pulse is the same as the interval between the π and final $\pi/2$ pulse, both paths accumulate the same amount of phase. This result is expected classically, and if classical action were the only effect and there was no phase difference between the paths, after the final $\pi/2$ pulse all of the atoms would be in the ground state.

In order to explain the phase difference between the two paths in the interferometer it is necessary to also consider the phase from the laser light as it excites or de-excites the atom. This calculation is also shown in Appendix A.1 and results in the well-known expression for the phase of the interferometer [1], [6], [7]. Another approach to deriving the phase difference is to consider the quantum mechanical behavior of the atoms; specifically, the evolution of the Hamiltonian that describe the atoms as they travel through the interferometer. Appendices A.2 and A.3 contain this calculation using two different formulations of the Hamiltonian. All three calculations in Appendix A show that the phase difference between the two paths in the interferometer is given by

$$\Delta\phi \quad = \quad kgT^2 \tag{2.1}$$

where k is the effective wavenumber of the light pulses, g is the acceleration due to gravity, and T is the time between pulses. I discuss this more in the context of Bragg transitions, but the effective wavenumber is approximately two times the wavenumber of the light that provides the momentum kick (exactly twice the wavenumber of light for Raman pulses), assuming a two photon transition. This is to say, $k_{eff} = 2k$, where $k = 2\pi/\lambda$ and λ is the wavelength of the light. With this phase difference, I also show in Appendix A that the probability of finding an atom in the excited state after it travels through the interferometer is given by

$$|\langle e\,|\psi_f\rangle\,|^2 \quad = \quad \frac{1}{2}(1 - cos(\Delta\phi)). \tag{2.2}$$

Here, $|\psi_f\rangle$ represents the wavefunction after the final $\pi/2$ pulse and $|e\rangle$ represents the excited state, such that $|\langle e|\psi_f\rangle|^2$ is the probability of measuring an atom in the excited state after traveling through the interferometer. Since the proportion of atoms in the excited state depends on the cosine of the phase difference between the paths in the interferometer, the

number of atoms in the excited state at the output of interferometer can precisely determine properties such as g. To demonstrate this and to quantify the potential sensitivity of these measurements, I take the derivative of the phase difference, (2.1) with respect to g, which gives

$$\frac{\partial(\Delta\phi)}{\partial g} = kT^2. \tag{2.3}$$

Rearranging and dividing both sides by g gives

$$\frac{\partial g}{g} = \frac{\partial(\Delta\phi)}{kgT^2}. \tag{2.4}$$

To calculate the sensitivity I assumed a conservative phase difference resolution of one part in ten and used an effective wavenumber corresponding to a wavelength of 461 nm light. Additionally I let time between pulses equal 140 ms, which is based on the travel time of atoms in a ten centimeter tower similar to one currently used at NPS (but for rubidium experiments). Putting these numbers into (2.4) gives

$$\frac{\partial g}{g} \approx 1.91 \times 10^{-8}. \tag{2.5}$$

This result shows that the ability to measure a phase difference of one part in ten in an atom interferometer translates to an ability to measure a change in gravitational acceleration of one part in approximately fifty million. This sensitivity is consistent for the single measurements reported in [1], who used cesium atoms and 160 ms between pulses. The sensitivity of atom interferometers also compares favorably with other methods for making precision measurements of gravity. A falling corner cube apparatus can have a sensitivity of $2x10^{-9}$ [1], but the setup is much more mechanically complex. Additionally the atom interferometer's sensitivity will increase with greater time between pulses, which is made possible in the 30 meter tower.

Atom interferometers designed to measure other parameters utilize different schemes, but the principle is the same: propagate an atom in a superposition of paths that accumulate different amounts of phase and then recombine them. To do this effectively, precise control of the atoms' starting position and momentum as well as allowing them to propagate

unperturbed except for the potential of interest is essential. In the next section, I discuss how atom interferometry experiments achieve this goal and are able to measure gravity, magnetic fields, and other phenomena.

2.2 Cooling and Trapping Atoms

Laser cooling of neutral atoms relies on the selective interaction of photons with atoms. When a photon has energy corresponding to an available electronic transition in an atom, the atom absorbs the photon, promoting one of its electrons to a higher energy excited state. Additionally, the photon transfers its momentum to the atom and the atom gains momentum in the amount of $\hbar k$ in the direction of the photon's motion. The atom will not remain in an excited state and will de-excite by emitting a photon with energy $\hbar\omega$ (where $\omega = 2\pi c/\lambda$ is the light's angular frequency) and momentum $\hbar k$. The atom de-excites back to its original state by emitting a photon with the same energy as the original incident photon. This photon is emitted in a random direction giving the atom a momentum kick in the opposite direction of emission. Since the laser beam imparts its momentum kick in a definite direction and the de-exciting photon imparts its momentum in a random direction, over a series of interactions the average momentum change is in the direction of laser propagation.

To use this effect to cool a cloud of atoms, lasers must be impart momentum changes that oppose the thermal motion of the atom. This requires lasers aligned in opposite directions along all three axes of motion (6 in total) as shown in Figure 2.2.

Additionally, the lasers must be tuned to have slightly less energy than the energy of the target transition being used to impart the momentum change. The reason for this so called "red detuning" is to control when the laser interacts the atoms. When the atom moves towards one of the laser beams it perceives the frequency of the photons to increase due to the Doppler shift. If the laser is red-detuned, the frequency shift is towards the peak of the absorption curve and the atom is more likely to absorb a photon and experience the corresponding momentum kick thus slowing down. Conversely when an atom has velocity away from the photons, the Doppler shift further decreases the perceived frequency making absorption less likely, which means the laser beam in the wrong direction will have less of an effect than the laser beam in the right direction. The specific wavelength of the lasers and amount of detuning depends on the target atom and the electron transition being used to drive the cooling. This effect occurs for a wide range of velocities and collects them into a narrow range of final velocity classes. Since the resultant spread in velocities is narrower than the initial spread, this effect can be termed "cooling."

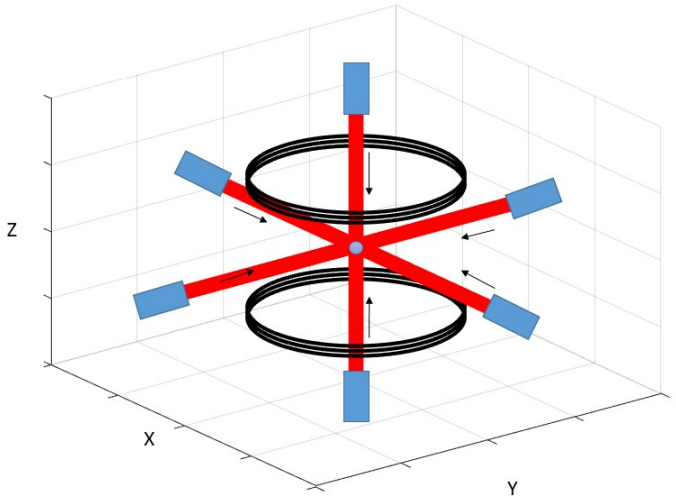

Figure 2.2. Orientation of lasers in a magneto-optical trap.

An excited atom will not always return to the original ground state when it emits a photon and de-excites. Instead it could transition to a different stable state or to a state that will take an impractically long amount of time to transition back to the original ground state. This is detrimental to the cooling process because the cooling lasers are setup to drive a specific transition. If an atom spends significant amount of time not in the either of the two states of the target transition, then it is not available for further cooling. As a result it will spend more time with a higher velocity and be able to escape the MOT before it is sufficiently slow enough to be trapped. Without accounting for this, the MOT is limited in how many atoms it can effectively trap. In order to counter this effect, MOT's utilize additional lasers to perform a process called repumping.

Repump lasers are selected and tuned to excite an atom that has decayed to an undesired state back to an excited state by promoting an electron to a higher energy level. From this new excited state the atom again de-excites by emitting a photon with the electron dropping to a lower energy level. If this lower energy level is the target initial state of the cooling lasers, then the atom is now available for further cooling. Repumping increases the efficiency of the MOT because it decreases the time for atoms to return to the target ground state.

The final temperature of a cloud of atoms in a MOT depends on the strength of the transition being used to transfer momentum from the lasers to the atoms. Once a target atom absorbs a photon and is in the excited state it is unavailable for further cooling until it de-excites. Each

transition is characterized by a frequency that describes how many times that transition can occur per second, which is the spontaneous emission rate and is equal to the reciprocal of the excited state lifetime. A higher spontaneous emission rate means the atom tends to de-excite faster and will be available for another cooling cycle more often. However, since the transition is occurring more often, the atom is also emitting photons in a random direction more often as it de-excites. The random direction momentum kick results in an effective heating mechanism. The final residual temperature, referred to as the Doppler cooling limit, is the balance between the laser cooling and the spontaneous emission heating and is given by

$$T_{min} = \frac{\hbar\Gamma}{2k_b} \tag{2.6}$$

where $\hbar$ is the reduced Planck's constant, Γ is spontaneous emission rate, which is also the linewidth of the transition given in radians per second, and k_b is the Boltzmann constant [8]. A transition that has a high spontaneous emission rate (and hence is spectral broad) is referred to as a "strong" transition. The advantage of using strong and broad transitions for cooling is that it is possible to quickly cool a large population of atoms, but as (2.6) shows, they result in a higher residual temperature. A narrower transition has a lower Doppler limit, but because the transitions happen less often the process takes longer and more atoms escape before reaching the final temperature.

Since different atoms have their own unique spectroscopy, each MOT will cool the atoms by driving transitions applicable for that atom. Therefore, the specific wavelengths of the cooling lasers as well as the number and settings of repump lasers depend on the atom species targeted in the MOT. I discuss the specific spectroscopy of strontium in Section 2.3.

Cooling atoms reduces their kinetic energy but does not confine them to a specific spatial position. In order to trap the atoms at the center of a MOT, two current carrying coils aligned in an anti-Helmholtz configuration create a magnetic field gradient. This configuration creates a field that is a minimum at the center of the trap and linearly increases radially outward. Figure 2.3 shows orientation of the currents and the magnetic field for a two dimensional slice of the MOT.

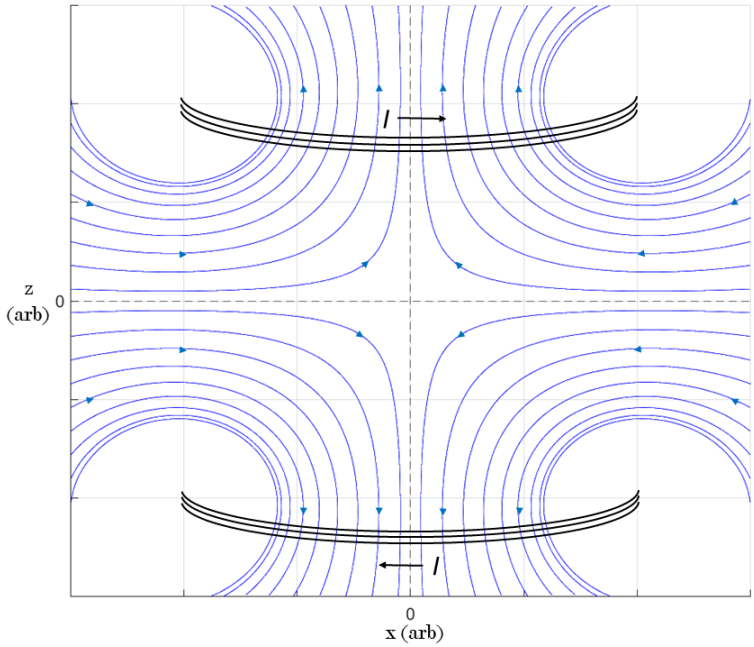

Figure 2.3. Magnetic field in a magneto-optical trap.

The presence of this magnetic field gradient causes Zeeman splitting of the spectral lines. This splitting reduces the energy difference between the ground and excited states as shown in Figure 2.4. Since the energy required for the transition decreases further from the center of the trap, the transition is gets closer to resonance with the red detuned laser light as the atom's displacement increases. Therefore the atom is more likely to absorb a photon from the cooling laser and be pushed back towards the center.

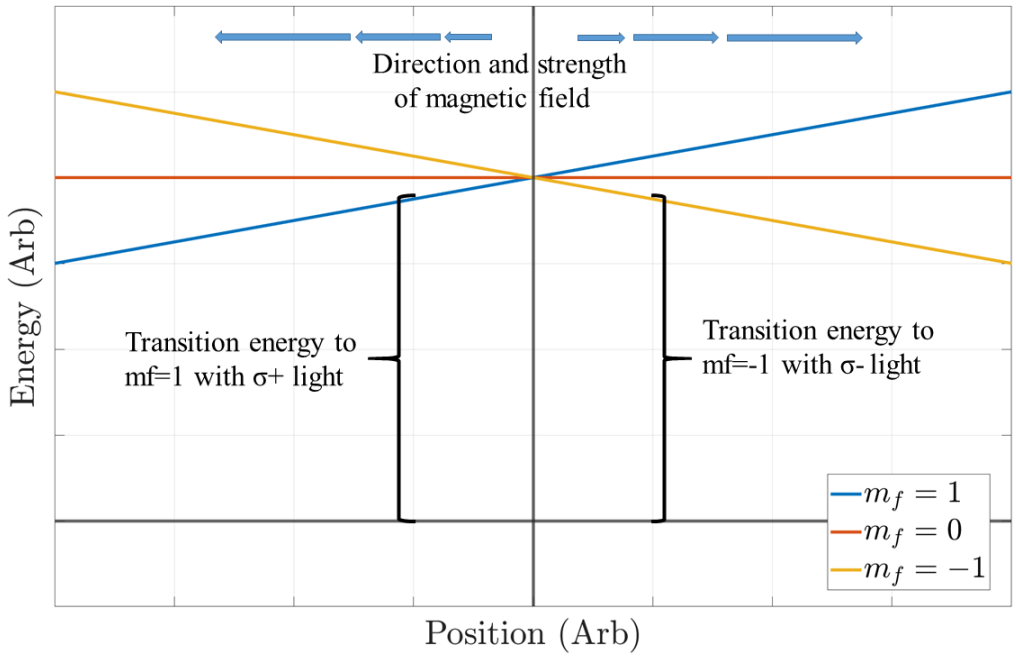

Figure 2.4. Effect of a magnetic field on transition energy. Adapted from [9].

By utilizing selection rules and polarization of the laser light, the MOT ensures displaced atoms are pushed back towards the center instead of away. For atoms displaced in the positive z direction (take its y and x position to be 0 for this example) from the center, Figure 2.4 shows that the Zeeman splitting brings the m_f=-1 transition closer to resonance. Only light circularly polarized in the σ^- direction can drive this transition due to selection rules and conservation of angular momentum. Therefore the displaced atom receives a momentum kick in the -z direction from the σ^- light and does not interact with the σ^+ light traveling in the positive z direction. Similar reasoning and selection applies for atoms displaced in other directions though it is important to consider the direction of the magnetic field for each case.

Overall, the MOT is an effective mechanism to produce a population of atoms for interferometry experiments. By capturing a large number of atoms, cooling them down to minimize their kinetic energy, and confining them to a small area, the MOT provides a known and well defined initial state for the experiments to make precision measurements.

2.3 Strontium

My thesis work focused on the setup for atom interferometry experiments in the planned 30 meter tower. These experiments will use strontium atoms. In this section I discuss the advantages and opportunities that strontium presents as well as the challenges.

The first advantage of strontium for atom interferometry is the absence of hyperfine structure. Hyperfine structure results from the different angular momentum configurations an atom can occupy. The total angular momentum, $\vec{F}$, of an atom is the vector sum

$$\vec{F} = \vec{L} + \vec{S} + \vec{I}, \tag{2.7}$$

where $\vec{L}$ is the electron orbital momentum, $\vec{S}$ is the electron spin angular momentum, and $\vec{I}$ is the nuclear spin angular momentum [10]. Therefore, the possible values of $\vec{F}$, depend on the electronic and nuclear structure of strontium. As a Group II Alkali Earth element strontium has an electron configuration of $(1s)^2(2s)^2(2p)^6(3s)^2(3p)^6(4s)^2(3d)^{10}(4p)^6(5s)^2$ that can also be written as $[Kr](5s)^2$ where [Kr] represents the electron configuration of Krypton, the previous closed shell Noble gas element on the periodic table [11]. This electron configuration means that strontium has two valence electrons that are paired in the 5s orbital. In the s orbital they have an ℓ quantum number of zero, meaning there is no net orbital angular momentum so $\vec{L}$ is always zero. Also since the valence electrons are paired, their individual $\vec{S}$ vectors will be anti-aligned, so the net spin angular momentum, $\vec{S}$ is zero. This means that in the neutral ground state, strontium has zero orbital and spin angular momentum.

The nuclear spin depends on the nuclear makeup of each isotope of strontium. A strontium nucleus has 38 protons but isotopes exist with 46, 48, 49, and 50 neutrons. For isotopes with even number of nucleons (protons and neutron) the antialigned spins will cancel in pairs and result in a value of zero for $\vec{I}$ [12]. Since these isotopes have integer spin, specifically zero, they are bosonic. For isotopes with an odd number of nucleons, the spins will not cancel and therefore the nuclear spin will be an integer multiple of $1/2$. The half integer value of spin makes these isotopes fermionic. Table 2.1, using data from [12] summarizes the relevant isotopes of strontium and their properties including their relative abundance and nuclear spin values.

Isotope	Abundance (%)	I	Species
^{84}Sr	.56	0	Boson
^{86}Sr	9.86	0	Boson
^{87}Sr	7.00	9/2	Fermion
^{88}Sr	82.58	0	Boson

Table 2.1. Properties of strontium isotopes. Data from [12].

The initial experiments in the 30 meter tower plan to use strontium 88, which is the most naturally abundant isotope at 83%. Since this isotope is bosonic, it has zero nuclear spin. Taken together with the orbital angular momentum and electron spin, strontium 88 provides the ability to work with atoms with zero total angular momentum in the ground state. Since there is zero total angular momentum, there is only one angular momentum configuration for the atoms, and therefore no hyperfine structure.

The absence of hyperfine structure is useful for atom interferometry because it minimizes the influence of magnetic fields to affect the motion of the atoms and, more importantly, the phase of the atomic wavefunction and thus the coherence of the system. With only one angular momentum configuration, $\vec{F}$=0, in the ground state, the atoms are not sensitive to the first order Zeeman effect but only to the second order Zeeman effect. Thus the atoms' susceptibility to Earth's or other magnetic fields is minimal, reducing phase noise in the atoms' wavefunction. As a result, there is no need to magnetically shield the interferometer significantly simplifying the experimental setup (although a single layer of shield vice three for the rubidium experiments is planned to reduce second order Zeeman effects).

The second main advantage of strontium is the availability of multiple cooling transitions. Using information from [12], [13], [14], [15], and [16], Figure 2.5 shows the spectroscopy of strontium. There is a small disagreement in the transition frequencies reported by these references. The transition frequencies shown in Figure 2.5 are from [13], which is published by the National Institute of Standards and Technology (NIST). This diagram defines the

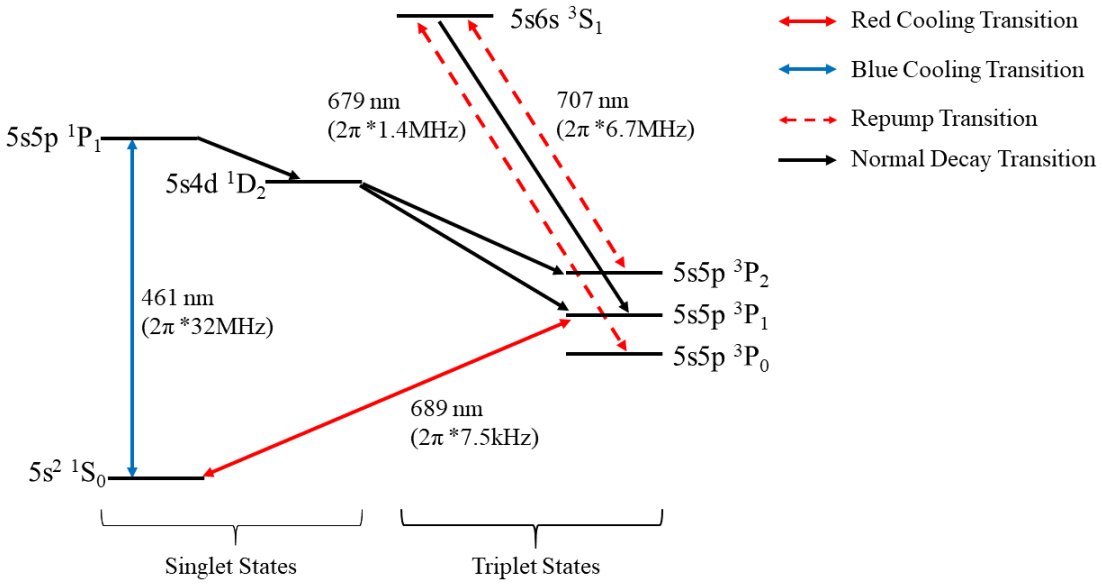

Figure 2.5. Spectroscopy of strontium.

usable cooling transitions as well as the number and wavelengths of repump lasers. For strontium there are two cooling transitions available, a "blue" one using 461 nm light and a "red" one using 689 nm light. As shown, these two transitions have two different linewidths. The blue transition between the ground $(5s)^2$ state and the singlet $5s5p\,^1P_1$ occurs at a frequency of 2π(32 MHz), so on average an atom will stay in the $5s5p\,^1P_1$ for 4.97 ns before transitioning back to the ground state. Inside a MOT using this cooling transition, every time an atom absorbs a momentum kick from a photon of this frequency it is unavailable for more momentum kicks and further cooling for approximately 4.97 ns. The Doppler limit for the lowest attainable temperature when using the blue transition is approximately 765 μK. Comparatively the red transition between between the ground $(5s)^2$ state and the triplet $5s5p\,^3P_1$ is much narrower with a linewidth of 2π(7.5 kHz), which results in a much lower Doppler limit of .18μK or 180 nK. However, using this transition, an atom will be unavailable for further cooling for an average of 21.2 μs after receiving a momentum kick from a 689 nm photon.

The advantage of the blue transition is that an excited atom quickly decays back to its ground state and spends more time available for further cooling. This allows a MOT to quickly capture a large number of atoms. However since the blue transition has a higher Doppler limit, the atoms will have a higher final temperature. The red transition has a lower Doppler limit so it can achieve a lower final temperature, but because the atoms spend more time in the excited state and are not available for cooling as often as the blue transition, the atoms will take longer to reach the Doppler limit, giving the atoms more time to escape the effective trapping region of the MOT, and resulting in a smaller final population of atoms in the MOT. To summarize, using just the blue a MOT would trap more atoms at a higher temperature while using just the red would trap fewer atoms at a lower temperature.

Since strontium has both of these transitions available, it is feasible to use them sequentially to trap a large population of atoms at a lower temperature. The MOT first uses the blue transition to trap and cool a large number of atoms at the higher Doppler limit temperature and then switches lasers to use the red transition to further cool the atoms in the trap. Since the atoms were already cooled (and trapped) by the blue transition they are less likely to leak out of the trapping region during the red transition phase.

The two repump transitions are at 679 nm and 707 nm. These are excited state transitions and they are necessary to expedite the return of an atom to the ground state when it decays into the branch starting with the $5s4d\ ^1D_2$ state vice the original ground state. These lasers are only necessary when using the blue cooling laser. It is possible to form a strontium

MOT without the repump lasers, however using the repump lasers increases the number of atoms in the MOT by up to a factor of ten [15]. Another group found that using just the 707 nm repump increased MOT population by a factor of four and that adding the 679 nm repump laser further increased the MOT population by a factor of ten [17]. Overall the repump lasers are important to optimize the strontium MOT and provide the largest possible atom number in the MOT to perform atom interferometry experiments.

Summarizing, the advantages of using strontium for atom interferometry are the absence of hyperfine structure that minimizes the effects of external magnetic fields and the presence of multiple cooling transitions that allows the experiment to start with more atoms at a lower temperature. These two features enable more precise measurements because of the increased signal from a larger number of atoms and decreased noise due in part to the magnetic field insensitivity. Atom interferometry depends on our ability to measure the population of atoms in the ground and excited state. Excessive dispersion of the atoms obscures the ability to make this distinction effectively.

There are two main disadvantages of using strontium. The first is a result of the very same lack of hyperfine structure in the ground state of bosonic strontium that we mentioned as an advantage in the preceding paragraphs. Experiments that utilize rubidium are able to differentiate between the ground and excited momentum states of the atoms because they coincided with different electronic states. Since bosonic strontium only has one ground state this type of differentiation is not possible. Furthermore, rubidium experiments transitioned the atoms between the momentum states and their corresponding electronic states via Raman pulses. Since strontium only has one ground state configuration Raman pulses are not possible. As a result, Bragg transitions are necessary to move atoms between the ground and excited states. I discuss this in greater detail in the next section, but Bragg transitions require spatial separation between ground and excited state atoms making limiting dispersion all the more important. The second disadvantage is related to the fairly narrow linewidth of the red cooling transition. With a linewidth of $2\pi(7.5\text{ kHz})$, the laser driving this transition has to be "linewidth narrowed", very precisely tuned and locked in order to be effective.

Strontium is useful for atom interferometry experiments because its properties enable more precise measurements. Due to its electronic configuration and nuclear structure the vast majority of natural occurring strontium atoms have no hyperfine structure. Additionally with two usable cooling transitions, strontium can be cooled to lower temperatures through normal Doppler cooling than other elements like rubidium. As a result, the phenomena

under study (gravity, magnetic fields, etc.) are the predominant influence on interferometer's output measurements rather than stray magnetic fields or dispersion of the atom cloud. However, using strontium for atom interferometry requires a different optical setup as well as Bragg transitions vice Raman transitions to transfer the atoms between momentum states. Since atom interferometry experiments at NPS to date used rubidium they also used Raman pulses. As a result, it is necessary to understand the setup and mechanisms of Bragg transitions for experiments with strontium.

2.4 Bragg Transitions

In this section I discuss the theory and mechanism of Bragg transitions as well the optical setup to implement them in atom interferometry experiments. For this section when I refer to strontium, I am considering the strontium 88 isotope that is bosonic and the most abundant naturally occurring isotope. As discussed in the previous section, the goal of a Bragg transition is to transfer an atom between a excited momentum state and a ground momentum state without changing its electronic state. The key relationship Bragg transitions leverage is the connection between the energy and momentum of an atom, given by

$$E = \frac{p^2}{2m}. \tag{2.8}$$

This relationship shows the amount of kinetic energy that corresponds to a given amount of momentum. The mechanism for changing momentum and energy in a Bragg transition absorbing and emitting photons. When an atom absorbs a photon, it transitions to an excited electronic state and gains energy $\hbar\omega$ and momentum $\hbar k$ from the incident photon. In order to coherently and sustainably keep an atom in excited momentum state a second laser stimulates emission of a photon from the atom while it is in the excited electronic state.

Bragg transitions require two counter-propagating laser beams in order to transfer the atom into a stable higher momentum state. The first, parallel to the direction of the desired momentum kick, provides photons that excite the atom. The second laser, anti-parallel to the direction of the desired final momentum, stimulates emission and de-excites the atom. Defining the momentum of the incident photon as $\hbar\vec{\boldsymbol{k}}_i$ and the emitted photon as $\hbar\vec{\boldsymbol{k}}_e$, the total change in momentum is $\hbar(\vec{\boldsymbol{k}}_i - \vec{\boldsymbol{k}}_e)$, which has a magnitude of $\hbar(|\boldsymbol{k}_i| + |\boldsymbol{k}_e|)$ since the two lasers are counter-propagating. The change in energy by absorbing and emitting these photons is $\hbar(\omega_i - \omega_e)$. If this change in energy from these photons matches the change in energy required for the corresponding momentum change given by (2.8), then the transition

is resonant and will occur [6], [18].

Figure 2.6 shows an example Bragg transition. The energy-momentum relation defined by (2.8) is shown by the blue curve. In this case the atom starts at the origin with zero momentum and kinetic energy. It gains energy and momentum by absorbing an incident first photon as shown by the upward red arrow. It then emits another photon losing energy and getting another momentum kick. The downward red arrow intersects the energy-momentum curve, which means that this transition is resonant and can occur. After the transition, the atom is left in a higher momentum state, but with its electrons in the original ground state.

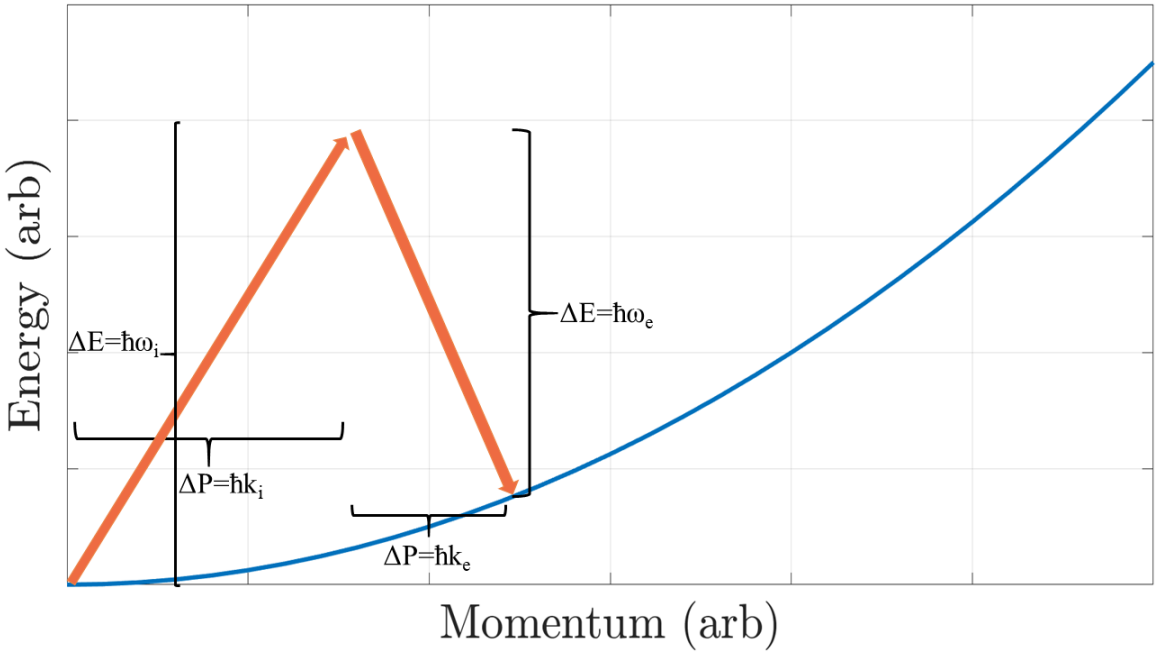

Figure 2.6. Example 2 photon Bragg transition.

The resonant condition for a Bragg transition is not limited to a two photon exchange between the two laser beams. The system could be setup such that the energy-momentum relationship is satisfied after absorbing and emitting multiple pairs of photons. If we let n be the number of pairs of photons the transition uses, then the total change in momentum is $n\hbar(|\boldsymbol{k}_i| + |\boldsymbol{k}_e|)$ and the change in energy is $n\hbar(\omega_i - \omega_e)$. Figure 2.7 shows a Bragg transition that is resonant for 5 pairs of photons. The advantage of using higher number photon transitions is that it imparts a greater momentum change, however this transition is much more complex and hence more difficult to implement.

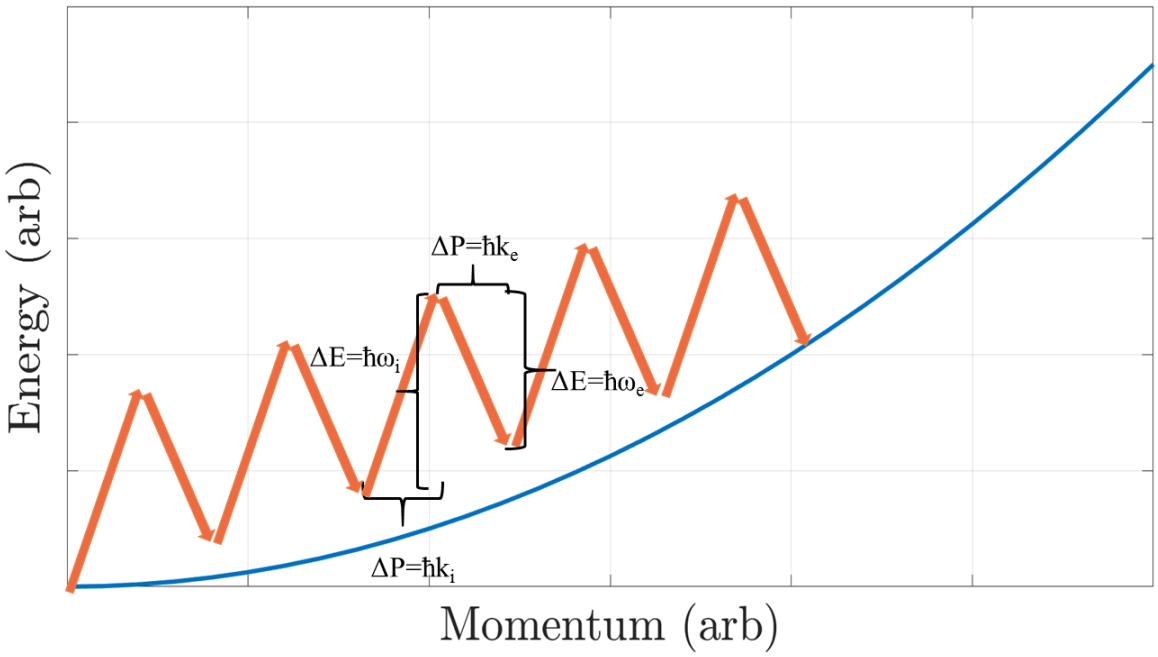

Figure 2.7. Example 10 photon Bragg transition.

Other groups have implemented Bragg transitions using two separate lasers, with different frequency tunings, each originating on one side of the trapped atoms and retro-reflecting the beams [3], [18]. One laser is tuned such that it interacts with the atom while traveling upwards, while on the way way back down it does not because the Doppler shift of the frequency moves it further from resonance. The other beam is tuned such that it is in resonance when the atom has upward velocity and thus stimulates emission from the atom while it traveling downwards. Together the two beams provide the desired momentum kick in the preferred direction. In the experiments in the 30 meter tower the atoms will be tossed upwards, so there must be a clear and unobstructed path. This means that for the Bragg laser it is practical to use fiber to put the source of one of the beams at the top of the tower removing the need for retro-reflection. With the laser sources separated, they can be tuned separately to account for the Doppler shift from the atoms motion and achieve the resonant relationship between energy and momentum. The specific strategy is still under consideration.

Bragg transitions are necessary for atom interferometry with strontium since there is no ground state hyperfine structure. The disadvantage of using Bragg transitions is the loss of the intrinsic tagging that comes with matching atoms in either the ground or excited momentum state to different hyperfine electronic ground states. For example, in rubidium experiments with Raman pulses, atoms in the excited momentum state are in a different ground state than atoms in the ground momentum state. With this distinction, by tuning a

laser to excite one of the ground states to another energy level and observing the fluorescence, it is possible to calculate the population of atoms in that state. With strontium and Bragg transitions the only way to resolve the populations of atoms in the ground and excited momentum state is to separate them spatially.

THIS PAGE INTENTIONALLY LEFT BLANK

CHAPTER 3:
Design, Operation, and Characteristics of the Optical System

In this chapter, I present the laboratory work to tune and lock all three lasers for the strontium atom interferometry experiments in the 30 meter tower. For my thesis I worked with the 461 nm blue cooling laser as well as the 679 nm and 707 nm repump lasers. The 689 nm cooling laser is still in the acquisition process but is not needed for the initial cooling and launch experiments. First, I outline several different operating schemes that I considered for this system of lasers. The overview includes considerations involving key pieces of equipment in the optical system. Next, I detail the optical setup I constructed to generate the feedback signal necessary to lock the repump lasers. The system I developed has the advantage of being compact because of the use of common optics and doesn't require an expensive wavemeter. Finally, I examine the characteristics and stability of the locking system output and how it responds to environmental factors.

3.1 Overview of Laser Locking System

I considered several strategies with the available equipment to develop the optical layout for use in locking the lasers needed to do strontium atom interferometry. In this section I present the key components of the system as well as their purpose and performance characteristics. I also discuss the strategies I considered for the laser stabilization scheme including the advantages and disadvantages of each.

The most important components of my system were the lasers themselves. As discussed with the spectroscopy of strontium, the MOT for experiments with strontium requires two cooling and two repump lasers. The 679 nm and 707 nm repump lasers in my experiment were diode lasers manufactured by Toptica Photonics and had rated output powers of 67 mW and 28 mW respectively. A Toptica Digital Laser Controller operated both of these lasers. This control box could receive feedback signals and independently adjust the output frequency for each laser. The 461 nm laser was manufactured by M-Squared Inc., and was significantly more complex than the repump lasers. It consisted of a pump laser that drove a Titanium:Sapphire (Ti:Saph) laser in the infrared range at about 922 nm. This 922 nm light then went through a nonlinear optical doubler that generated the necessary 461 nm light. The 689 nm cooling laser is not yet on hand.

The next key piece of equipment was a High Finesse WS8-30 Wavelength Meter, referred to simply as a wavemeter. The wavemeter could monitor the wavelength of up to eight separate lasers through an attached switch that took fiber inputs and cycled between them. The measurement time and thus the time to cycle through each laser depended on the number of lasers being monitored as well as their input intensity. The greater the intensity of the laser, the faster the wavemeter made an effective measurement. In addition to monitoring wavelengths, the wavemeter could also compare the measured wavelength to a reference value and generate a feedback signal based on standard proportional, integral, differential (PID) control for up to 8 lasers. The wavemeter displayed measurements with precision of 1 femtometer and had a listed absolute accuracy of 30 MHz [19]. At the wavelengths for strontium experiments this corresponded to an accuracy of roughly 50 femtometers. The wavemeter was useful for initial tuning of the lasers and characterization of the locking, but was not strictly required to operate the locking scheme I developed.

The final major component of the frequency locking system was a reliable frequency standard to use as a reference for both the lasers and the wavemeter. The best possible standard was the atoms themselves and the specific target transition of the system. The reason I used the atoms themselves is that these transitions,as properties of nature, did not drift or need calibration. The locking system used the laser's interaction with a population of strontium atoms to develop a reference standard signal for the lasers. A Photronics hollow cathode lamp (HCL) provided the source of strontium atoms for the experiment. This lamp consisted of an optogalvanic cell that with an applied current generated a population of strontium atoms with valence electrons in both the ground and excited states. Generating a population of atoms in the excited state was important because the repump transitions for strontium are excited state. Without this population the it would not be possible to observe any absorption at the repump frequencies.

Figure 3.1 shows the first and most straightforward strategy for frequency locking the lasers. In this scheme, the wavemeter measures the frequency of each laser and provides a feedback signal to each laser's controller. This setup requires a calibration standard for the wavemeter to reference. I used a locked 780 nm laser from another experiment in the Quantum Sensing Lab as the reference. This scheme has the advantage of requiring the least amount of optical setup, but it is limited by the accuracy and sample time of the wavemeter. It also requires the purchasing of an expensive wavemeter if one is not readily available. Additionally since this setup uses laser light from another experiment, the strontium setup would not be completely independent, which is not desirable.

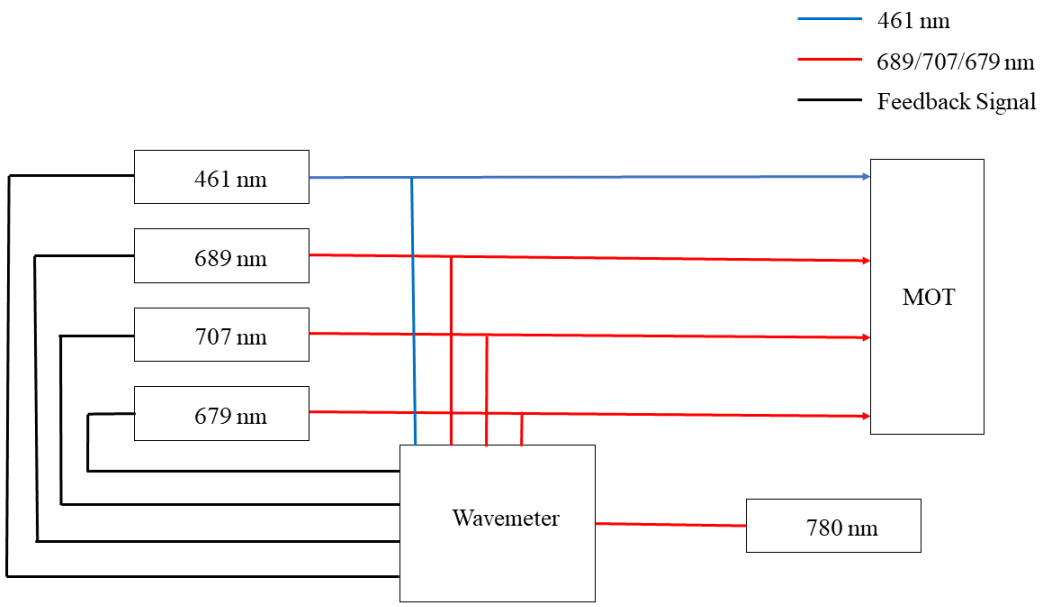

Figure 3.1. Laser stabilization using only a wavemeter.

Figure 3.2 shows the next scheme considered. In this setup, the optical system generates a feedback signal based on the interaction of a portion of the 461 nm light with the strontium in HCL as mentioned above. This signal calibrates the wavemeter and then the wavemeter samples, feeds back to and controls the two repump lasers. The first advantage of this setup is that the system has a strontium reference that is independent of other experiments. The second advantage is that this scheme requires minimal optical layout, which serves to minimize the optical setup although more equipment and alignment is required than the scheme depicted in Figure 3.1. The disadvantage with this setup is that it is subject to the timing limitations of the wavemeter.

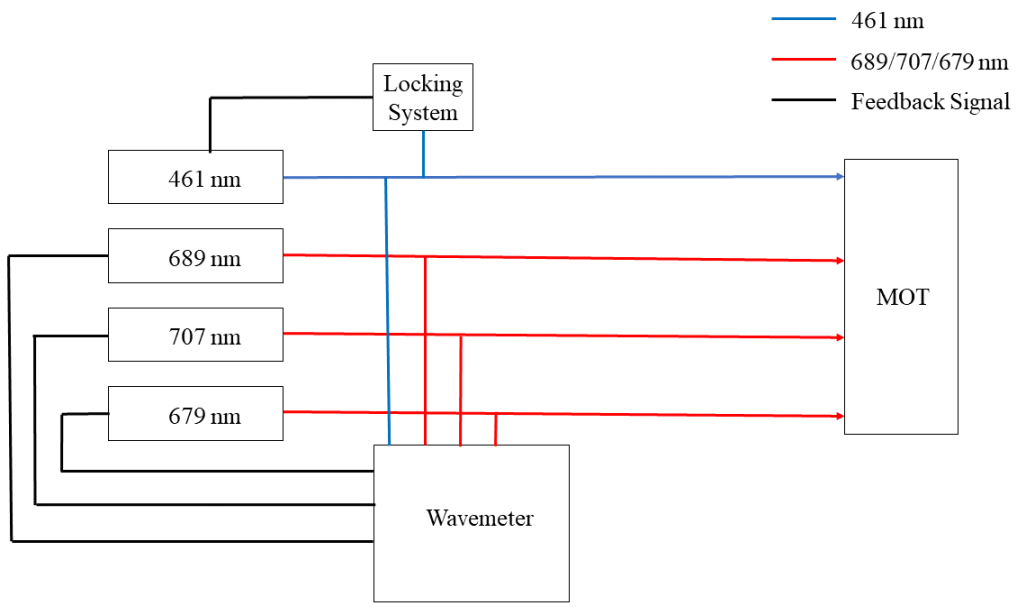

Figure 3.2. Laser stabilization using 461 nm standard and wavemeter.

In starting to work with this optical set up, the 461 nm laser started to experience technical difficulties. During setup and alignment there were several issues with the pump laser and it had to be returned to the manufacturer and replaced. When the replacement pump laser came and I proceeded with the alignment and installation, I noted limited performance and efficiency with the system. The manufacturer eventually sent a technical representative who corrected several issues but performance was still limited and eventually deteriorated. In early January 2022, the entire system was returned to the company for a factory alignment and mounting. As a result the 461 nm cooling laser was not available for an extended period of time and I had to pursue another strategy.

Figure 3.3 shows the setup I pursued. In this scheme, the wavemeter monitors the outputs of the lasers and assesses performance of the system. This system has the advantage that each laser is locked to its respective transition and the wavemeter is used only as a device to characterize the locking. Since all lasers are locked to an atomic reference, one can also serve as a frequency standard for the wavemeter. The main disadvantage is that it is very complex and requires a lot of optical setup and alignment.

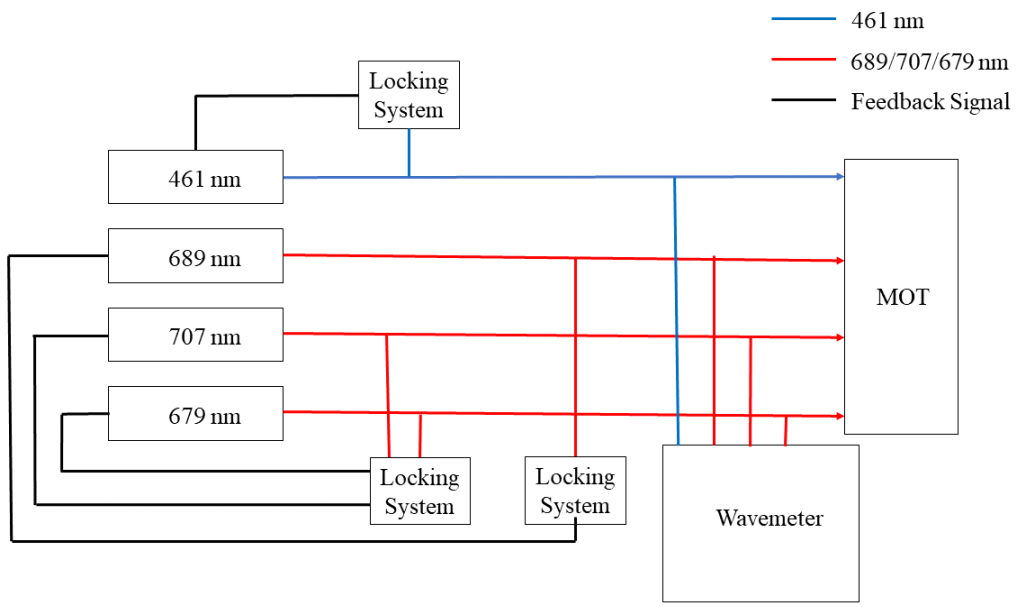

Figure 3.3. Laser stabilization using multiple atomic references.

An important advantage of this new scheme is that both of the repump lasers share the same locking system, which saves space and components and also allows investigation of the interactions between various excited states of strontium. In the next section I present the locking system box in greater detail and characterize performance of the lasers and the system.

3.2 Dual Laser Stabilization System Setup

The physical principle that motivated the design of this system is commonly referred to as saturated absorption spectroscopy. This technique is used ubiquitously throughout the NPS Quantum Sensing Lab with rubidium cells and involves sending a probe laser beam through a sample of atoms to a detector. The closer the beam's frequency is to resonance with the atoms, the more light is absorbed and the less reaches the detector. Adding a pump beam travelling anti-parallel to and intersecting the probe excites the atoms out of their initial state making them unavailable for absorption by the probe beam, and allowing more transmittance to the detector. This effect is most pronounced for atoms with no velocity component in the direction of either beams. When plotted against frequency this signal consists of an absorption dip with a Doppler-free feature near resonance. A second probe beam travels through a different region of the sample that has no pump beam to another detector. This detector shows only a Doppler-broadened absorption dip. Subtracting the probe-only signal from the pump-and-probe signal reduces the impact of Doppler broadening of the transition

and results in a Doppler-free signal.

Standard saturated absorption was not practical for my experiment. In the HCL, required because the repump transitions are excited states, most of the atoms were very near the electrode. As a result, I focused the beams to maximize the chance of interaction between the light and the atoms. Focusing multiple beams in different focal spots in the geometrically constrained space of the HCL would have been impractical. Additionally the amount of absorption from the repump transitions was very small and barely detectable against the larger laser intensity signal.

The locking system I developed for the strontium repump lasers used an intersecting pump-probe setup similar to standard saturated absorption as well as a lock-in detection method that identified the absorption signal against the laser background and and amplified it. I modulated the pump beam rapidly, which rapidly changed the population of atoms available for absorption by the probe. Therefore, the absorption signal of the probe laser oscillated at the same frequency as the pump modulation. Mixing the detector output with the control signal modulating the pump laser in a lock-in amplifier filtered all extraneous signals and generated a useful signal to lock the lasers.

Figure 3.4 shows a diagram of the dual laser locking setup. The output of each laser was coupled into a 99/1 fiber splitter that sent one percent of the power to the wavemeter for monitoring and analysis and ninety nine percent through a collimator and into the rest of the system. After the collimator, the light first passed through a polarizer. The purpose of the polarizer was to maintain a constant input polarization for each laser. The lasers next passed through a half wave plate and polarizing beam splitter (PBS) combination that defined the split of laser power between the pump and probe branch. A PBS directed the light into each branch by passing the the horizontal component of light straight through and deflecting the vertical component of light. By rotating the half wave plate, the relative weights of horizontal versus vertical components and hence the splitting ratio could be adjusted. In the 707 nm laser arm of the setup, horizontally polarized light went into to the pump branch and the vertically polarized light to the probe branch. Conversely, the 679 nm probe was horizontally polarized and the pump was vertically polarized. For the 707 nm laser, the power in the probe beam was 240 micro-watts while in the pump beam power was 458 micro-watts. The 679 nm laser used 30 micro-watts in the probe beam and 3 milliwatts in the pump beam.

The probe beams for the 707 nm laser and 679 nm laser traveled anti-parallel through the cell. Lenses on each side of the cell focused each beam into a small volume and then

recollimated the laser fields. Additionally the beams traveled as close as possible to the walls of the cell where the population of excited state strontium was the greatest. Since the two probe beams had crossed polarization, a PBS after the HCL directed the beams to their respective detectors and limited the potential for cross talk between the two lasers. The output of the photodiode detectors were sent into lock-in amplifiers.

Steering mirrors directed each pump beam around the HCL and through an acousto-optic modulator (AOM). When the AOM was on, it used radiofrequency energy passing through a crystal to deflect a portion of the laser light, called the first order beam. The undeflected portion of the light, called the zeroth order beam, passed straight through. When the AOM was off, all light passed straight through unaffected as the zeroth order beam. A square wave signal at frequency f_c, called the chopping frequency, went from a function generator to the AOM intensity control, cycling the intensity of the deflected beam on and off. An iris blocked the zeroth order beam in each branch and steering mirrors directed the first order beam into the cell where it intersected the probe beam. When the AOM was on the first order beam was present and provided pumping in the HCL, however when it was off the first order beam was completely extinguished removing the pumping. Since the AOM cycled at f_c, the pump beam was modulated at this same frequency as well. The pump and probe beam for each laser were not overlapped, rather the pump beam passed through at an angle and intersected the probe at one point. Irises on the other side of the cell blocked the pump beam and prevented light from one wavelength reaching the detector for the other wavelength.

The photodiode signal and the chopping signal with frequency f_c connected to a lock-in amplifier where they were mixed together. The lock-in amplifier picked out the portion of the signal that was modulated at the chopping frequency, f_c. The portion of the signal that oscillates was the difference between the probe only and pump-probe absorption profiles. The lock-in amplifier output went to a PID controller that generated a feedback signal and sent it to the repump lasers' controller to stabilize laser frequency.

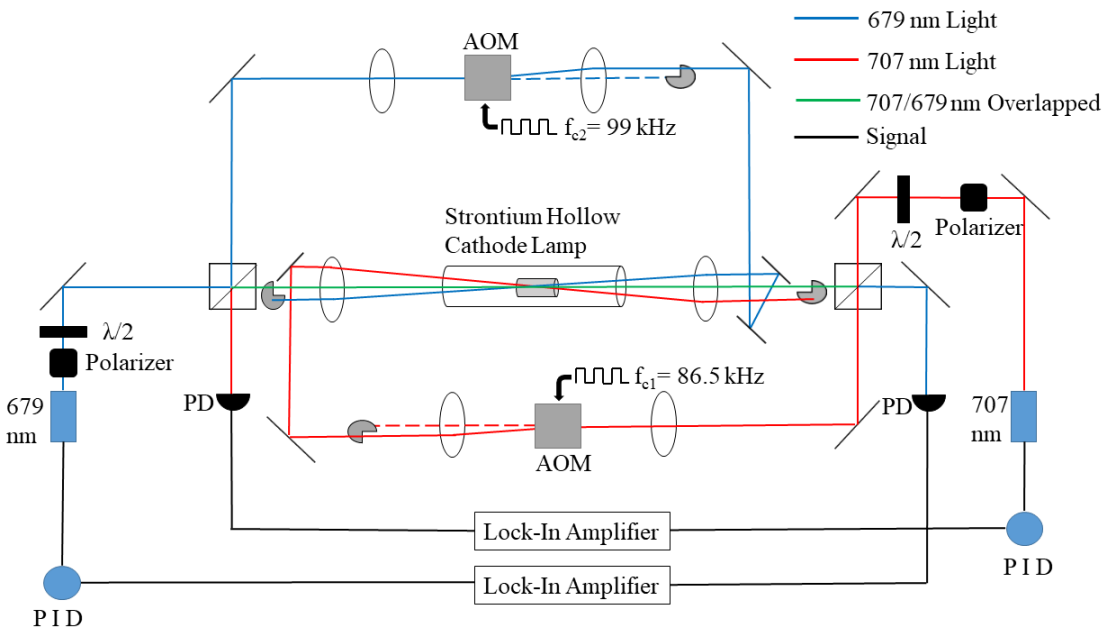

Figure 3.4. Locking system line diagram.

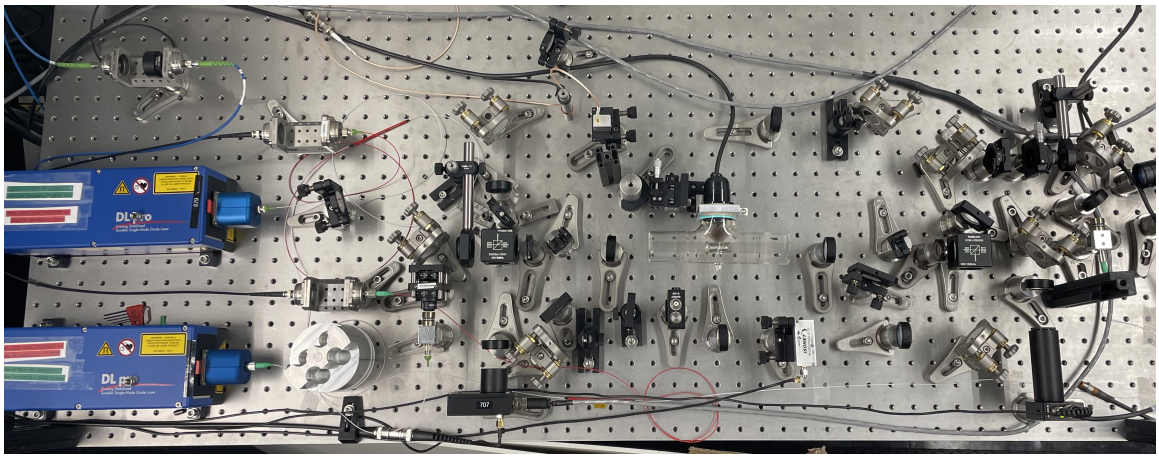

Figure 3.5. Locking system photograph.

The programming of the PID adjusted the laser frequency to maintain the lock-in amplifier output at a specifically chosen setpoint. The setpoint was not the peak of the signal, but rather a point on side of the peak that was ideally a consistent frequency offset away from the peak. If I used peak locking, there would have been ambiguity when correlating a change in lock-in amplifier output voltage to a change in laser frequency. If the system attempted to maintain the peak voltage and the laser drifted, output voltage would decrease, but the system would not know whether to raise or lower the laser frequency to return the output to a maximum.

I used side locking rather than peak locking to remove the ambiguity. Choosing the setpoint on the side of the peak, meant that when output signal voltage was less than the setpoint value, laser frequency was too low, and when it is above the setpoint value, laser frequency was too high. If the laser frequency drifted sufficiently far from the setpoint that it is past the chosen setpoint on the other side of the curve then the ambiguity returns. Past this point the output would be below the setpoint, and the system would try to raise laser frequency when instead it should lower it. The difference in frequency from the lock point on one side of the curve to the equivalent output on the other side is the upper bound of the systems effective locking range. The final experimental setup will use AOMs to shift the frequency of the light going to the MOT from the side locking setpoint back to resonance. Figure 3.6 shows an example locking laser lock setpoint as well as the effective capture range of the system.

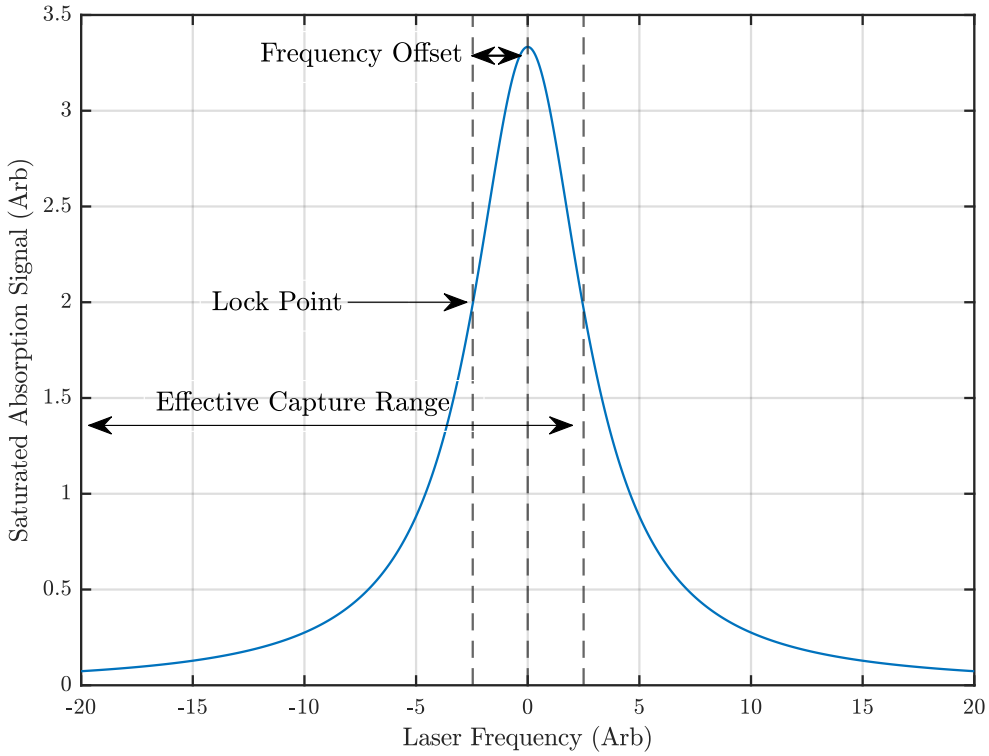

Figure 3.6. Example locking system setpoint.

3.3 Characteristics of the Locking System Output Signal

The laser locking system was based on generating a signal from the absorption profile of the 707 nm and 679 nm transitions in strontium. The stability and accuracy of that signal determined the effectiveness of the laser locking system. In this section I present the characteristics of the output signal from the locking system.

Figure 3.7 shows the output of the photo-detectors for the 707 nm and 679 nm lasers respectively prior to any processing by the lock-in amplifiers. Additionally the solid vertical line and two dashed lines on these plots shows the nominal transition wavelength and uncertainty values from [13]. To generate these plots, I scanned each laser over a range of frequencies (and corresponding wavelengths) covering the resonant frequency of the transition and averaged 256 sweeps. I also used the MATLAB smoothing function to clean up the data. I performed this measurement first with just the probe beam and again after introducing an un-modulated pump beam. Since laser power was not constant over a frequency scan, I fit a curve to the result and subtracted out the effects of the power ramp. Next, I normalized the curves to their respective maximum value. Finally I subtracted the pump-probe signal from the probe only signal. This difference is the signal that the lock-in amplifier pulled out from the background noise. Also the difference signal here is what I use for comparison to the lock-in amplifier output for each laser.

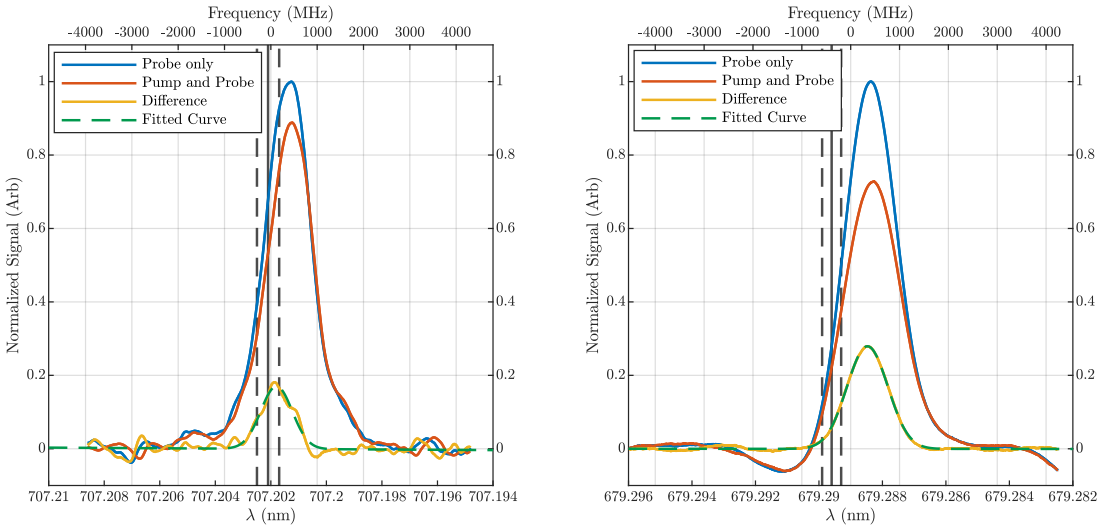

Figure 3.7. (a) 707 nm detector Signals. Frequency axis indicates frequency difference from 707.202 nm (b) 679 Detector Signals. Frequency axis indicates frequency difference from 679.289 nm.

One important aspect of these signals that normalization obscured was the relative strength of the two transitions. Prior to normalizing the peak signal for the 707 nm transition was approximately 33 times greater than the 679 nm. This meant that the 679 nm signal required significantly more amplification to generate a usable signal and had a smaller signal to noise ratio.

Figure 3.8 shows the output of the lock-in amplifier for various settings of the lock-in amplifiers integration time constants. These figures show that as the time constant increased the noise in the signal decreased, for the reason that the lock-in amplifier integrated out more noise from the signal. However, increasing the time constant meant that the signal updated slower, which meant that the locking feedback signal would have been slower to update. For each time constant the 679 nm signal was always noisier than the 707 nm signal. This was due to the relative strength of the transition as discussed above.

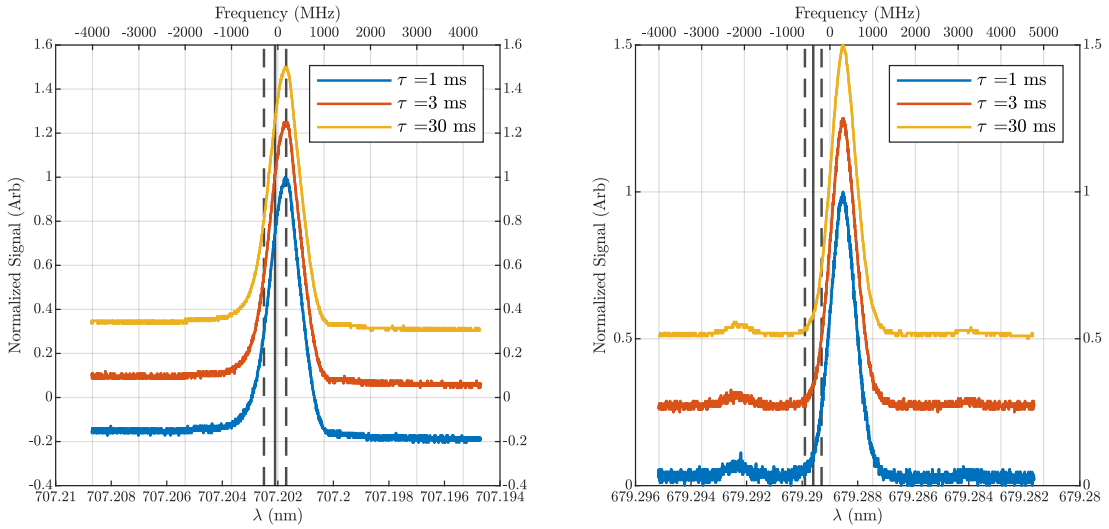

Figure 3.8. (a) 707 nm lock-in signals with offsets added for clarity. Frequency axis indicates frequency difference from 707.202 nm (b) 679 nm lock-in signals with offsets added for clarity. Frequency axis indicates frequency difference from 679.289 nm.

To analyze the characteristics of the signal I fit a Gaussian of the form

$$Signal = Ae^{\frac{-(f-B)^2}{C^2}} + D + Ef \tag{3.1}$$

to the probe only signal and the difference signal from Figure 3.7, as well as the the lock-in amplifier outputs shown in Figure 3.8 for both transitions as a function of frequency. I also tried a Lorentzian fit, but found that the Gaussian function fit the data better. The fact that the

Gaussian function fit better indicates that the signals had significant Doppler broadening. Table 3.1 shows the results of these fits. The fit results for each of the three time constants shown in Figure 3.8 were very close as expected, therefore the result reported in the table represents the average value of that parameter for the three lock-in amplifier curves for each respective laser. The fit for 707 nm difference signal had the lowest R^2 value, which was due to higher noise levels in the signal particularly in the wings.

Gaussian Fit Results of Observed Data						
Parameter	A	B	C	D	E	R^2
707 Probe Only	.9866	374.2	700.4	.01473	$-6.459x10^{-7}$	.9937
707 Difference	.1703	122.3	479.8	-.0002285	$-7.055x10^{-7}$	.9020
707 Lock In	1.1320	142.2835	474.9	-.1646	$-6.3813x10^{-6}$	.9968
679 Probe Only	1.011	425.8	731.6	-.007155	$4.177x10^{-7}$	.9929
679 Difference	.2794	343.1	591.2	-.0002138	$-5.601x10^{-8}$	.9978
679 Lock In	.9376	311.5	426.4	.0279	$-9.0282x10^{-7}$	.9968

Table 3.1. Gaussian fit results from observed data.

For comparison I analyzed data from [17] and [20] for the 707 nm and 679 nm transitions respectively. [17] performed single laser stabilization to the 707 nm transition while [20] performed spectroscopy of various strontium transitions including the 679 nm transition. Both of these references provided curves for a probe only and pump-probe signal. I extracted and interpolated the data for both curves, and subtracted them to produce a difference signal. Figure 3.8 shows the results of this analysis.

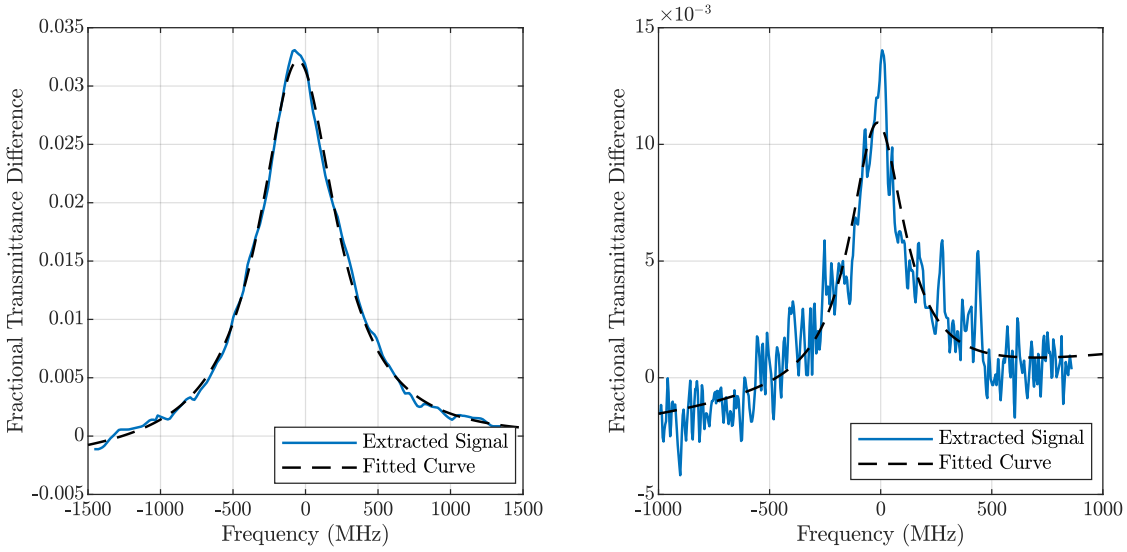

Figure 3.9. (a) 707 nm pump-probe difference signal using data extracted from [17]. (b) 679 nm pump-probe difference signal using data extracted from [20].

I fit these curves with Lorentzian and a Gaussian functions of frequency. For the data from these references I found the Lorentzian function of the form

$$Signal = \frac{A(\frac{B}{2})}{(\frac{B}{2})^2 + (f - C)^2} + D + Ef \tag{3.2}$$

better fit the data for both transitions. I expected a Gaussian to fit the data better, given that the extracted data from both sources show a linewidth broader than the natural linewidth; however, without more details regarding how the two groups conducted their experiments and processed their data, I cannot definitively explain why the Lorentzian fit better than the Gaussian. Table 3.2 shows the results of the Lorentzian fit for each transition. The curve of the 679 signal was very noisy and as a result its fit had the largest amount of error. Again, this result was expected due to the relative weakness of the transition.

Lorentzian Fit results of Reference Data						
Parameter	A	B	C	D	E	R^2
707 Difference	10.84	642.7	-52.81	-.001505	$5.574x10^{-7}$	.9972
679 Difference	1.716	299.5	-15.34	-.0005151	$-1.284x10^{-6}$	.8784

Table 3.2. Lorentzian fit results of difference signal calculated with data extracted from [17] and [20].

Table 3.3 summarizes the important parameters of each of these curves and signals. There are two important notes to mention for this data. First, [13] gives nominal values, denoted as

λ_0, for the two transitions as well as their uncertainties as wavelengths in air. However, the wavemeter outputs and exports vacuum wavelengths, though it can display air wavelengths. Therefore, I converted the values and uncertainties in [13] to vacuum wavelengths using indices of refraction of 1.000275754 and 1.000276041 for the 707 nm and 679 nm values respectively. I calculated these values by comparing the wavemeter's displayed vacuum wavelength and air wavelength in the range of the 707 nm and 679 nm transition. An error analysis showed that the error in the the index of refraction was insignificant compared to the error in the nominal wavelength.

Another important note is that in order to make a consistent comparison between the reference curves of [17] and [20] that fit better to Lorentzian functions and my data that fit better to Gaussian functions I considered the linewidth of the transition to be the full width at half maximum (FWHM) of the signal peak. For the curves from [17] and [20] this was the value of B from the Lorentzian fit. For the curves from my data, I calculated the FWHM using the equation

$$FWHM = 2C\sqrt{ln(2)} \tag{3.3}$$

where C was the from the Gaussian fit.

Parameter	707 nm	679 nm
λ_0 (converted from [13])	707.2021*	689.2896*
λ_0 (Probe Only)	707.2014	689.2883
λ_0 (Difference)	707.2018	689.2885
λ_0 (Lock-In)	707.2018	689.2885
Linewidth (Probe Only) (MHz)	1166	1218
Linewidth (Difference) (MHz)	799	985
Linewidth (Lock-In) (MHz)	791	710
Linewidth (Reference) (MHz)	643* [17]	299* [20]

Table 3.3. Characteristics of spectrum signal. * indicates the value in the table was calculated from data in the listed reference as previously discussed.

The detector and lock-in amplifier signals for both the 707 nm and 679 nm transitions showed an offset from nominal wavelength. For the 707 nm laser this offset was approximately .34 picometers or 200 MHz, which is within the uncertainty of [13]. For the 679 nm laser it is approximately 1.1 picometers or 700 MHz, which was outside of the uncertainty of [13]. This offset was not a particular concern for the purpose of laser stability, but it does warrant further examination. One possible source of the offset was the dynamics of the HCL. The

electric fields inside this lamp that produced the population of strontium atoms could cause a shift in the nominal transition wavelength. The first step to investigate this is to use the 461 nm laser once it is refurbished and operational to perform similar spectroscopic measurements with the 30 meter tower strontium source once it arrives. This source does not have the same fields as the HCL and, in fact, is a very pristine environment within which to do the experiment. The next step is to perform similar spectroscopic measurement with the 461 nm laser and the HCL and compare to the results with the strontium atom source. This will determine if the offset is caused by the HCL, the accuracy of the wavemeter, or some other effect.

As discussed, the atoms themselves were the ultimate standard for the transitions, and this signal was derived from the laser interaction with those atoms. The presence of the signal showed that my setup elicited a response from the atoms. Additionally the observed peak offset was well within the capacity of the final experiment to correct with an AOM.

The second important parameter to analyze is the linewidth of the transition. As expected, the linewidth of the probe-only signal was broader than the difference signal and lock-in output for both transitions. Also as expected the difference signal and lock-in signal were very similar for the 707 nm transitions. For the 679 nm transition the difference signal was broader than the lock-in signal. Given the amount of averaging and processing that went into generating the difference signal, the fact that the lock-in output was narrower indicated how effective the lock-in amplifier is. The 679 nm signal was very small and was barely visible at the detector output. It is reasonable to conclude that filtering and boosting the signal via the lock-in amplifier yielded a better result.

The lock-in amplifier outputs for both transitions were broader than the signals calculated from [17] and [20] but they were on the same order of magnitude. For the 707 nm signal the difference was noticeable but not significant. For the 679 nm signal the difference was more pronounced. One reason was that the team in [20] used an HCL with a special Neon and Xenon filler gas that suppressed Doppler broadening and increased the number of atoms in the target state. The HCL in my setup did not have this filler gas. Additionally my setup was optimized to maximize the signal to noise ratio to generate a feedback signal for frequency stabilization rather than perform precision spectroscopy. Due to the level of noise, the extracted signal from [20] would not be suitable for frequency stabilization. The broadening present in the lock-in amplifier output of my system was a necessary trade-off to generate a signal with a high enough signal to noise ratio to produce an effective feedback signal. The fact that all linewidths, both from my observations and the extracted reference

data, were significantly larger than the natural linewidths of each transition shows that each experiment operates in a power and Doppler broadened region. The conclusion from comparing these linewidths is that the lock-in amplifier output reasonably compares with other efforts to produce similar signals.

Overall, these results showed that the laser locking system generated an effective signal for frequency stabilization of the 679 nm and 707 nm lasers. The signal for both transitions reflected the atoms' response to the lasers and allowed an appropriate locking setpoint at a frequency to make an effective MOT.

3.4 Signal Stability

Any change that affected the setpoint of the locking system also affected the output frequency of the laser. Therefore it was necessary to examine how the feedback signal drifted over time and responded to environmental factors. To assess the long term stability of the locking system signal signal I continuously scanned the laser over a period of approximately 20 hours and recorded the output of the lock-in amplifier. I performed this test with a previous iteration of my system design, and the results informed several changes and improvements.

Figure 3.10 shows the results for the 707 nm and 679 nm laser signals respectively. The 679 nm signal was more noisy than the 707 nm signal, but this was expected and consistent with previous results. Both of these figures also showed that the over the course of the data run the peak amplitude of the signal as well as the location relative to the center of the scan drifted significantly. The reason the location of the peak drifts was that the laser itself is drifting. The amplitude of the frequency scan was constant, but the central frequency drifted, which showed in this data as the location of the peak drifting.

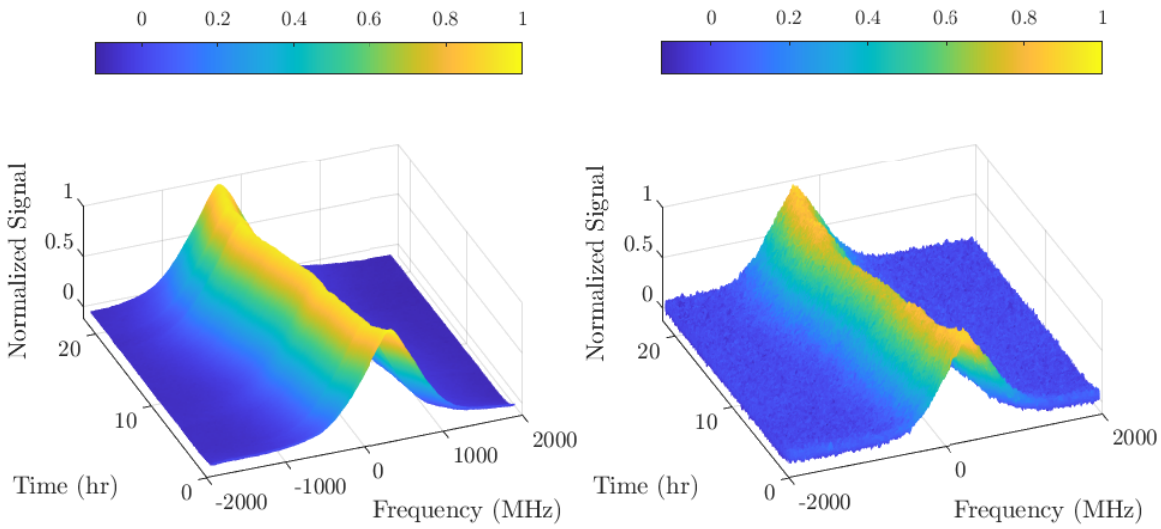

Figure 3.10. Signal spectrum over time for the (a) 707 nm signal and (b) 679 nm signal.

Figures 3.11 through 3.14 plot normalized peak signal, central frequency drift, frequency offset for a locking setpoint of 65 percent of the peak height of the first spectrum, and lab temperature for this data run for the 707 nm signal and 679 nm signals. I measured this data with all components of the system warmed up with the exception of the lock-in amplifiers. The reason I did not warm up the lock-in amplifier prior to this data run was that I suspected it had a significant warm-up time relative to the rest of the setup and I wanted to confirm that observation. As mentioned above, the central frequency drift was caused by the drift of laser frequency as it scanned, which further demonstrated the need for frequency stabilization. The normalized peak signal and frequency offset plots reflected the shape and stability of the signal as well as how the locking system setpoint relates to the final target frequency for the experiment. The frequency offset plot showed how far laser frequency would be from target frequency if the PID feedback and control was perfectly effective. This is the frequency change that the final AOM would correct before the laser is sent to the MOT. If the system and the signal were totally stable, the curves for normalized peak and frequency offset would be constant horizontal lines.

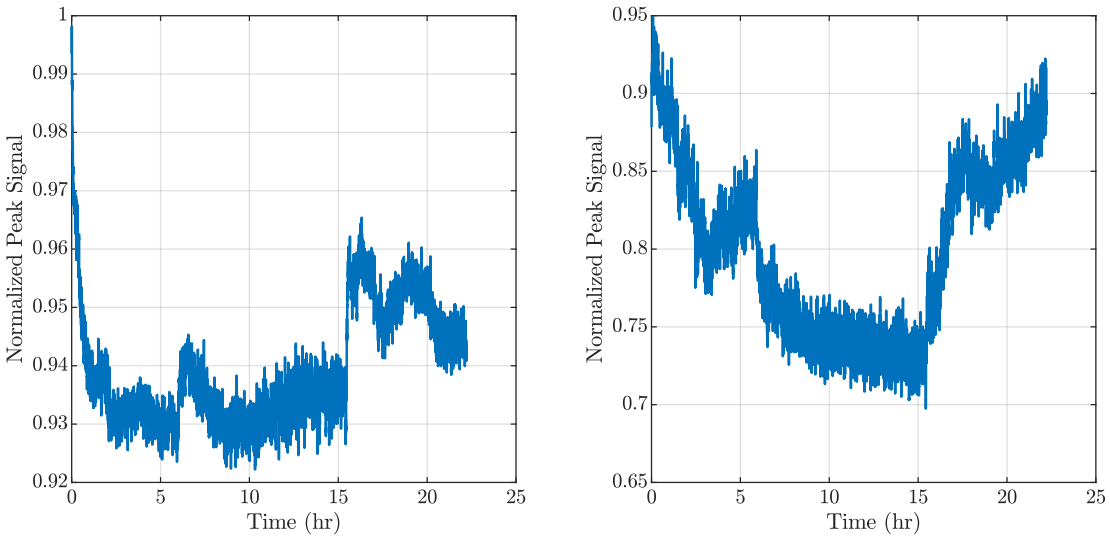

Figure 3.11. Normalized peak for the (a) 707 nm and (b) 679 nm signals.

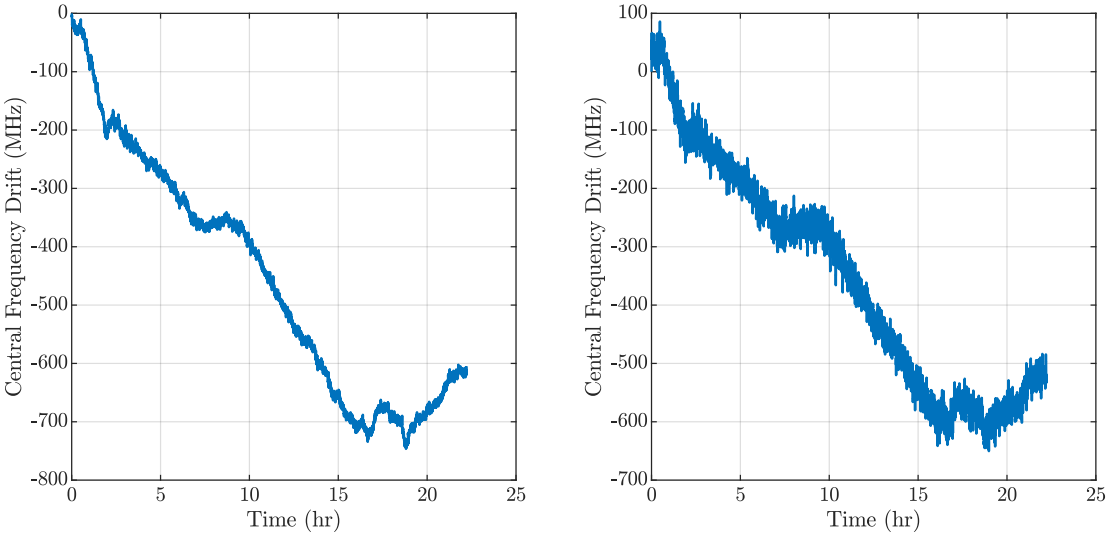

Figure 3.12. Center frequency over time for the (a) 707 nm and (b) 679 nm signals.

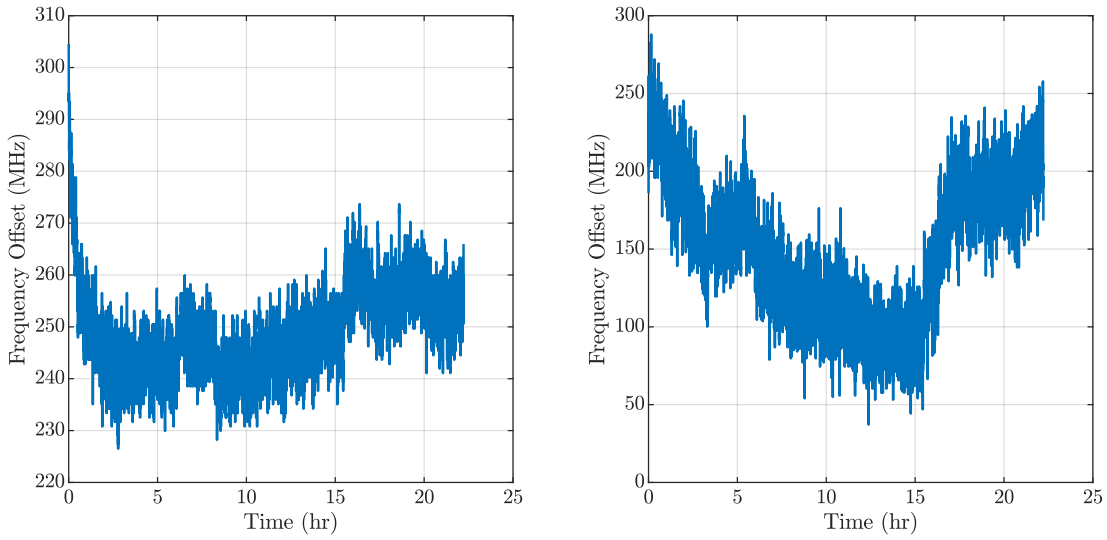

Figure 3.13. Frequency offset over time for the (a) 707 nm and (b) 679 nm signals.

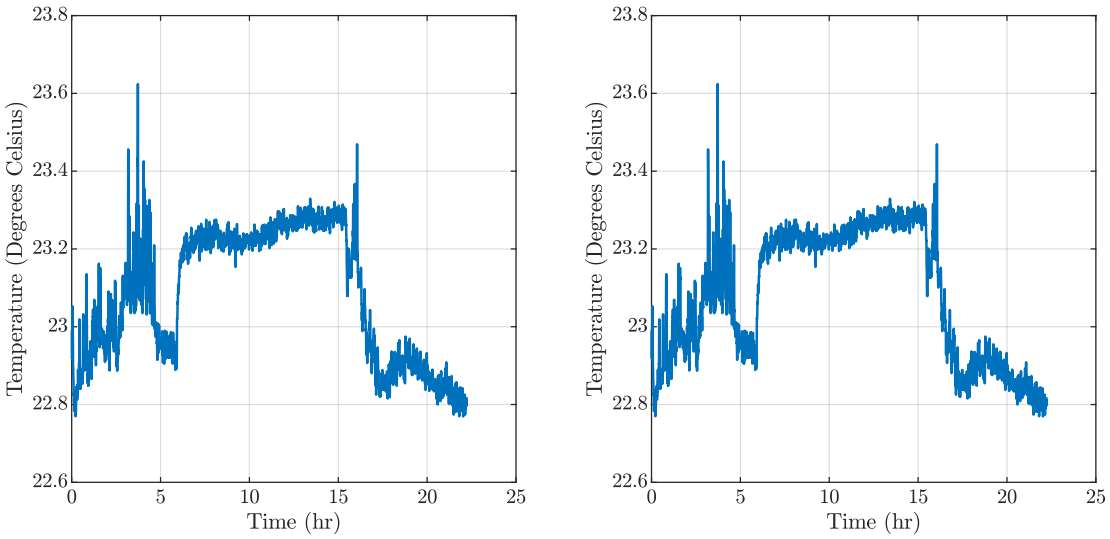

Figure 3.14. Laboratory temperature during data run. Repeated for clarity.

The normalized peak signal and frequency offset plots tracked with each other for each laser. They also roughly tracked with temperature in the lab and major jumps in the data roughly correlated with cycling of the heating ventilation and air conditioning (HVAC) unit that controls temperature in the lab. The immediate drop in the peak signal was due to the lock-in amplifiers warming up and reaching steady state. To address this issue I ensured the lock-in amplifiers were on and warmed up before using the system. The initial warm-up period has the most pronounced drift, but the changes were still substantial over other time periods. For example, between hours 10 and 15 the frequency offset changed by approximately 15 and 25 MHz for the 707nm and 679 nm lasers respectively. During this

interval there was no sudden event such as HVAC turn on, and the system was responding to changing ambient temperature. The conclusion from this data was that the locking system was susceptible to thermal drifts that those drifts significantly affected the locking system setpoint and thus the laser frequency output.

To mitigate these effects I took several actions. First, I attached the fibers carrying the laser light to the optical table or other metal structures to act as a heat sinks and minimize thermally induced polarization rotations in the fiber. This was particularly necessary for the 707 nm part of the system because polarization maintaining fibers splitters for this wavelength were unavailable. Additionally, I changed the mount of the HCL from a 3D printed mount to a machine metal mount for greater thermal resistance and stability. Furthermore, I installed cardboard barriers around the optical setup to provide insulation.

Looking ahead to the final experimental setup for atom interferometry in the 30 meter tower, the optical system will be at the bottom of a hollowed out elevator shaft. This area is a lot smaller and thus will be easier to climate control and maintain a constant temperature. As result the final experiment will be further insulated from the impact of thermal drifts and effects.

CHAPTER 4:
Results, Performance, and Future Work

In this Chapter I present the results of my experiment and the performance of the laser locking system. I first establish a baseline by operating the lasers without any feedback or control. Next I present how the lasers perform under the control of the locking systems and compare the results to the baseline. Finally I discuss these results, analyze their implications, and outline the next steps to improve performance and develop the complete optical system for strontium atom interferometry.

4.1 Locking System Performance

In order to evaluate the effectiveness of the locking system, I used the drift of each laser running with no control or feedback as a baseline. For this analysis, I turned on both lasers and used the wavemeter to measure the frequency of each laser. The wavemeter output a vacuum wavelength for each laser. I converted this wavelength to frequency and then subtracted the mean value for the data run. A 780 nm laser calibrated the wavemeter as previously described before taking data, but not during the run. The HCL and locking system were on and running during this data run, but the laser controller was not using the feedback signal.

Next I used the locking system to generate a feedback signal that I sent back to the lasers. For this data run, I used a 3 ms time constant on the lock-in amplifiers for both the 707 nm and 679 nm lasers. Additionally, I set the laser controller to adjust piezo voltage to control frequency based on feedback from the locking system.

Figure 4.1 plots the frequency of each laser versus time for both the locked and unlocked case. I also used the MATLAB `rmoutliers` function to remove outliers from the data. For the locked case this removed 67 data points (.2% of the total) from the 707 nm data and 226 data point(.63% of the total) from the 679 nm data. For the unlocked case this function removed zero data points (0% of the total) from the 707 nm data and four data points (.01% of the total) from the 679 nm data. For both lasers there was a significant drift in the unlocked case. The locked data showed that the locking system did cause some high frequency oscillations but significantly reduced the drift.

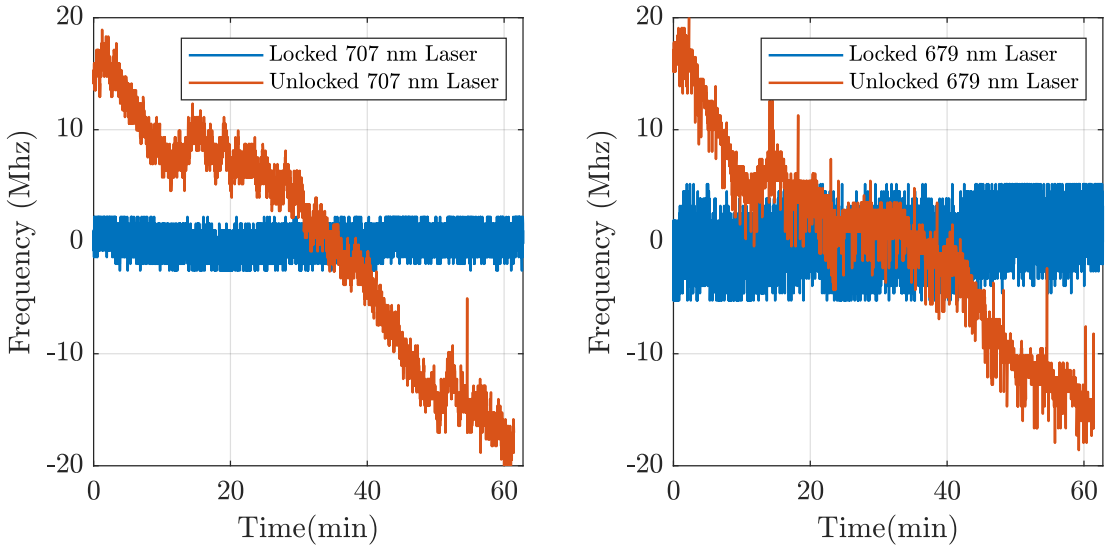

Figure 4.1. Frequency over time for the (a) 707 nm laser and (b) 679 nm laser.

Figure 4.2 plots the Allan deviation (ADEV) for various time constants for the locked and unlocked case for both lasers. See Appendix B.1 for an explanation of Allan deviation. I estimated the ADEV uncertainty for each time constant by dividing the ADEV by the number of data points to which each time constant averages the original set [21]. At longer time constants, more data is averaged into fewer points, therefore the uncertainty is larger, which is standard for ADEV curves. At the longest time constant the bottom range of uncertainty extended below zero. Since Figure 4.2 uses a logarithmic scale the lower bound on the uncertainty can not be shown.

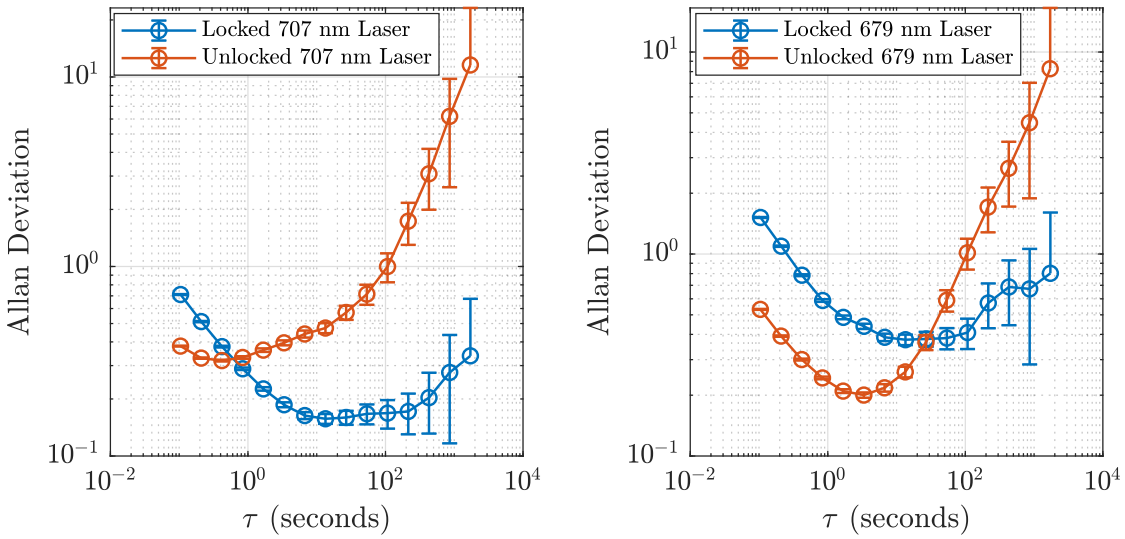

Figure 4.2. Allan deviation for various time constants for the (a) 707 nm laser and (b) 679 nm laser.

Figure 4.3 shows the noise spectrum of the lock-in amplifier output for each laser when it is locked and unlocked. At lower frequencies the locking system reduced the magnitude of the noise for both lasers. This effect was much more pronounced for the 707 nm laser, which makes sense since the locking system performed better for that laser. For the 679 nm laser, locking the laser did induce some higher frequency noise which was consistent with the results shown in Figure 4.1. In terms of laser performance, the reduction of low frequency noise and the associated drifts was more important than the introduction of the high frequency noise oscillations.

There were two other notable results in this data for the 707 nm laser. First for both the locked and unlocked case, the lock-in amplifier output had a noise peak at approximately 900 Hz. Also the spectrum is much more constant with increasing frequency compared to the 679 nm spectrum, which falls off at higher frequencies. These characteristics of the spectrum did not significantly affect the frequency stability of the 707 nm laser. Overall the noise spectrum plots show that the locking system effectively reduced low frequency noise and counteracted long term drifts. Also, the light from these lasers is used for the repump transitions, which have less stringent locking requirements than the cooling transition.

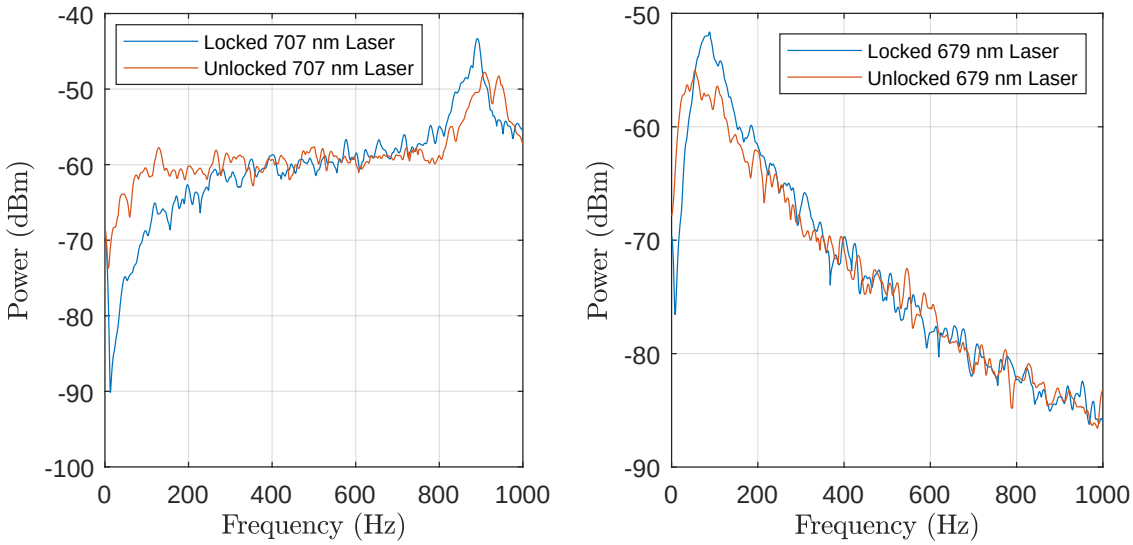

Figure 4.3. Noise power spectrum for the (a) 707 nm laser and (b) 679 nm laser.

Table 4.1 summarizes the key performance parameters for each laser for the locked and unlocked case. The standard deviation (σ) of the frequency distribution is the key measure of how tightly the laser was locked and whether it will be effective in driving the target transition (see Appendix B). This data shows that for both lasers the σ was tighter when locked than unlocked. For the 707 nm laser the observed σ of .86 MHz was significantly

less than the 6.7 MHz natural linewidth of the transition, 1.4 MHz. The σ for the locked 679 nm laser was improved from the unlocked case, but it was on the order of the natural linewidth of that transition. This was not ideal for the 679 nm laser, but it is possible to compensate and make a MOT by increasing the Rabi Frequency by using higher laser power.

For both lasers the locked case had a higher ADEV at shorter time constants due to the increase in high frequency oscillations from the locking system. However, the minimum time constant at which the minimum ADEV occurs was higher indicating that the locking system effectively reduced the long term frequency drift of both laser. For the 707 nm laser the minimum ADEV for the locked case was less than the minimum ADEV for the unlocked case. This was another indication that the system effectively reduced drift. With small drifts, the higher time constants averaged out more of the deviation caused by noise. For the 679 nm laser the minimum ADEV for the unlocked case was less than the locked case. This means that the increased time constant did not average out the additional noise from the locking system before the drift became the main source of deviation. However the fact that the locked ADEV stayed significantly below the unlocked ADEV as higher time constants indicates that the locking system was still effective at reducing drift.

Parameter	707 nm		679nm	
	Locked	Unlocked	Locked	Unlocked
Range (MHz)	4.80	39.56	10.40	39.98
σ (MHz)	.86	10.21	1.98	8.37
Min ADEV (MHz)	.16	.32	.38	.20
Min ADEV τ (s)	13.41	.42	13.47	3.35

Table 4.1. Stability parameters of the locked and unlocked 707 nm and 679 nm lasers.

For comparison, [17] performed a similar experiment to lock a laser to the 707 nm transition only and reported that the noise in their system led to frequency oscillations 1.7 MHz root mean squared. The σ of .86 MHz for the one hour run compares favorably with this value. I could not find a similar effort for the 679 nm transition.

Another important performance characteristic for the locking system is how long it can maintain a lock. To evaluate this I performed a 5 hour data run with the locking system stabilizing both lasers. Figures 4.4 and 4.5 show the results for this data run. For both lasers the σ was larger than for the shorter run. For the 707 nm laser the σ 1.72 MHz compared with .86 for the one hour run. For the 679 nm laser the σ was 2.48 MHz compared with 1.98

for the one hour run. Over a longer data run the system is more susceptible to drifts. For the 707 nm data, the frequency drifts had a cyclic behavior. However the system maintained the lock through these drifts with reasonable performance. As discussed previously, when the system is in its final location for strontium atom interferometry it will be easier to control temperature and mitigate these drifts.

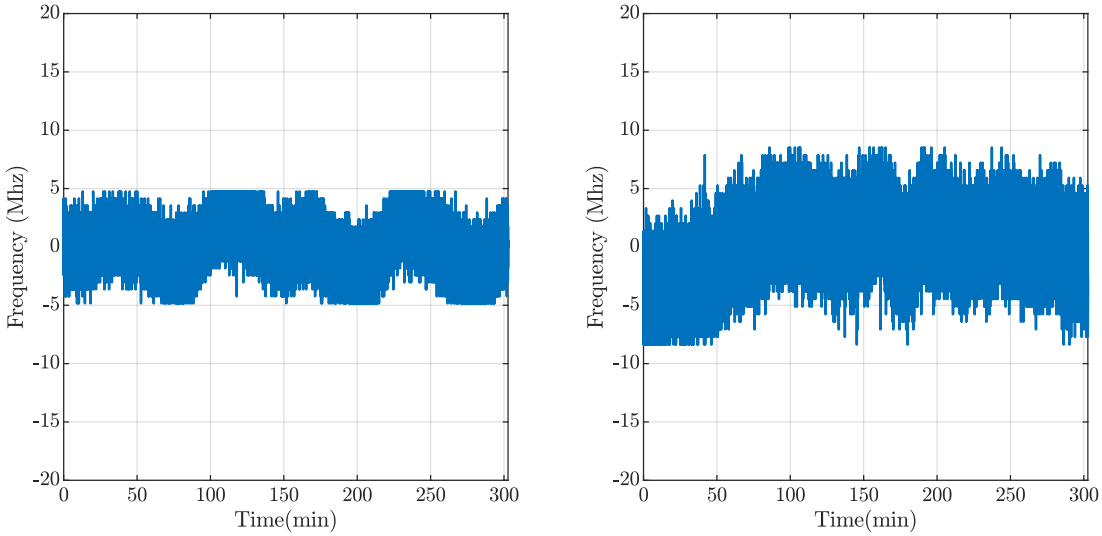

Figure 4.4. Frequency over time for a five hour data run for the (a) 707 nm laser and (b) 679 nm laser.

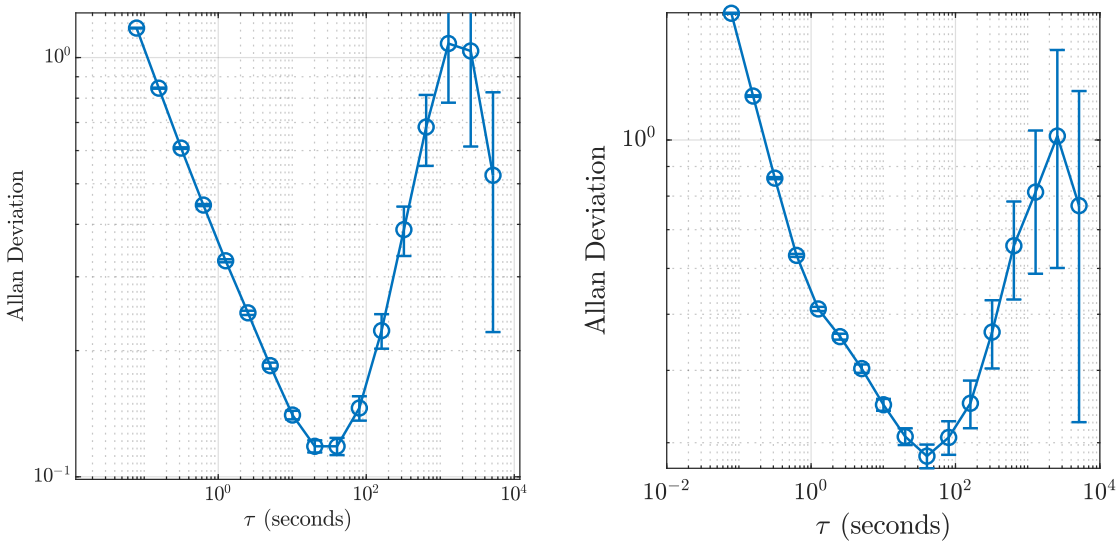

Figure 4.5. Allan deviation for various time constants for the (a) 707 nm laser and (b) 679 nm laser.

The locking system significantly improved the stability of both the 707 nm and 679 nm lasers. The system performed better for the 707 nm laser, but this was expected due to the small magnitude of the 679 nm signal. The locking system demonstrated the capacity to reduce the frequency spread of the laser to a value comparable to the natural linewidth of each transition, or significantly less in the case of the 707 nm laser. Additionally, it reduced the impact of long term frequency drifts. Finally, the system maintained an effective lock over an extended time interval. Overall, the data showed that the laser locking system stabilized laser frequency well enough to make a MOT.

4.2 Future Work and Improvements

The laser locking system I developed demonstrated the ability to effectively stabilize laser frequency. However as work continues to build out the experimental setup for strontium atom interferometry there will be an opportunity to further improve the performance and accuracy of the laser locking system. In this section I outline the future work and next steps to make the laser locking system more effective.

As discussed previously the laser locking system was susceptible to thermal drifts. These drifts affected the reference signal that the optical system generated as well as the lasers themselves. I took steps to mitigate these effects in the lab space of the setup, but the move to the final location offers an opportunity to improve temperature stability. The optical system supporting the strontium experiment will be in a recess below the 30 meter tower. This area is significantly smaller than the current lab space and will be much easier to temperature stabilize. With more stable ambient environmental conditions the reference signal will also be more stable and able to better lock the laser.

Another area to improve the performance of the locking system is the method in which the feedback signal adjusts laser frequency. In the previous data runs the feedback was aligned to change the piezo voltage of the laser in order to adjust frequency. The controller also offers the option to adjust frequency via the laser current as well as the laser temperature. The temperature control is a very slow feedback mechanism and not suited for addressing high frequency oscillations. Through the development of the locking system, I found that feeding back to the current via the controller produced similar results to feeding back to the piezo. Another option exists to feedback directly to the current via a connection on the laser itself. This option potentially offers much higher bandwidth. The downside is that it is a more complex setup and bypasses some of the current limits the laser controller provides. If a tighter lock is needed to support the experiments in the 30 meter tower then exploring

a laser lock via this method is warranted.

The final option to improve the stability of the two repump lasers is to either use the MOT itself or the strontium beam that loads the MOT. In fact, the source has a window designed in it for exactly that purpose. Once the strontium source is on hand and the rest of the optical system is in place, it will be possible to tune the settings of the feedback system in order to optimize the number of atoms in the MOT. Overall the atoms and MOT provide another practical reference for system performance.

The ultimate measure of system effectiveness is the capacity to drive the target transition and make a MOT. The dual laser frequency stabilization system effectively locked the lasers for this purpose, but there are opportunities to further optimize the system and improve performance as development continues.

THIS PAGE INTENTIONALLY LEFT BLANK

CHAPTER 5:
Conclusion

My thesis work was a meaningful contribution to the continued development of atom interferometry experiments at the NPS Quantum Sensing Lab and beyond. These contributions were both theoretical and practical in nature. My thesis provided a base of knowledge for working with strontium, excited state transitions, and Bragg transitions as well as an effective and necessary system for making precision measurements with atom interferometry.

From a theoretical perspective, in the background calculations of Appendix A, I used three different methods to calculate the phase difference of an atom interferometer that were consistent with themselves and the literature in the field [1], [6], [7]. By independently considering the phase due to laser pulses, the non-commutivity the ground and excited states Hamiltonians, and gravity as a time dependent momentum correction, I provided three paths to understand the theoretical underpinnings of an atom interferometer. Having these all worked out in one place is useful for future calculations involving different atom interferometer configurations. Depending on the context of a specific experiment one method of calculation may be more amenable than another. In addition my thesis involved the initial consideration of Bragg transitions for experiments at NPS. The discussion of Section 2.4 is particularly useful for the design of future experiments with strontium in the 30 meter tower.

More practically, the optical system I designed demonstrated the ability to simultaneously frequency stabilize two repump lasers for making a strontium MOT using fairly inexpensive components in a compact layout. My system successfully reduced the frequency spread of both lasers, minimized long term drifts, and maintained a lock over a long period of time through ambient condition changes. Additionally since my system used strontium atoms as the reference standard, the frequency to which the system locks is easily tuned to maximize the laser's ability to drive the target transition. Also, the Quantum Sensing Laboratory team gained valuable experience working with strontium, excited state transitions, and HCL's. This work was a successful step in developing strontium experiments at NPS because it provides tuned and stable repump lasers to maximize the amount of strontium atoms available for atom interferometry.

The 30 meter tower at NPS will be collaborative and interoperable with researchers at other institutions. Therefore it is necessary to document the development process and

performance parameters of the supporting systems. The data from Chapter 4 is especially important for all potential stakeholders to understand as they devise specific experiments for the 30 meter tower.

Systems like the one I developed are important enablers for atom interferometry experiments, but this particular system has several important characteristics that make it relevant for both future experiments at NPS as well as the wider community. One important factor is that my design achieves the desired frequency stability for both lasers simultaneously with only one strontium HCL. This minimizes the amount of optics, equipment, and space required for the system. This is significant for making the setup for these experiments more practical, affordable, and (most importantly for the Navy) usable in the field. Additionally while my design used a wavemeter to setup the system, rough tune the lasers to the transition frequency, and monitor laser stability while under lock, it is not in principle necessary. After finding an appropriate frequency range to scan over the target transition, the system I designed is easily capable of performing the laser lock without the wavemeter. The wavemeter is significantly expensive so methods that perform key functions for atom interferometry experiments without one, make the science more accessible.

In conclusion, my experiment successfully demonstrated a method to sustainably and practically frequency stabilize multiple lasers for strontium atom interferometry experiments. There is opportunity to further improve the system as development on the 30 meter tower continues, but the techniques and processes I used are effective for research at NPS and beyond. From a theoretical and practical perspective the work of my thesis was an important contribution to effort to use atom interferometry to make precision measurements.

APPENDIX A:
Background Calculations

In this Appendix, I calculate the phase difference between the two paths of the atom interferometer described in Chapter 2. First, I consider the phase due to classical action of atoms moving through a gravitational field as well phase from laser interactions with the atoms. Next, I perform the analysis using two different formulations of the Hamiltonian and use a quantum mechanical approach to determine the phase difference. I show that the phase difference as well as the output of the atom interferometer is the same for three different approaches. Additionally my results were consistent with other literature in the field [1], [6], [7].

A.1 Interferometer Phase via Classical Action and Laser Interaction

The following calculation uses a similiar one from [4] as a guide. I start with the action of the atom moving through a potential along a given path,

$$S = \int_{t_1}^{t_2} \mathcal{L}\, dt \tag{A.1}$$

where $\mathcal{L}$ is the Langrangian and given by:

$$\mathcal{L} = \frac{1}{2}m\dot{z}^2 - mgz \tag{A.2}$$

where

$$z = z_0 + v_0 t - \frac{1}{2}gt^2 \qquad \text{and} \tag{A.3a}$$

$$\dot{z} = v_0 - gt \tag{A.3b}$$

So the Lagrangian becomes

$$\mathcal{L} = \frac{1}{2}mv_0^2 - 2mv_0 gt + mg^2t^2 - mgz_0. \tag{A.4}$$

Evaluating the action integral

$$S = \int_{t_0}^{t_1} \mathcal{L}\, dt = \left[\frac{1}{2}mv_0^2 t - mv_0 g t^2 + \frac{1}{3}mg^2 t^3 - mgz_0 t\right]_{t_0}^{t_1}. \tag{A.5}$$

I define the time immediately after the $\pi/2$ pulse to be t_0=0. At this moment, along the upper path the atom received a momentum kick and has a transverse velocity, v_o. The lower path did not receive a momentum kick so its initial transverse velocity is 0. Both paths have a starting position 0 and propagate through the gravitational potential in this state to time t_1. Therefore the action along each path up to time t_1 is

$$S_{upper} = \frac{1}{2}mv_0^2 t_1 - mv_0 g t_1^2 + \frac{1}{3}mg^2 t_1^3 \qquad \text{and} \tag{A.6a}$$

$$S_{lower} = \frac{1}{3}mg^2 t_1^3. \tag{A.6b}$$

The next step is to evaluate the Lagrangian and action integral for each path after the π pulse. The form of the Lagrangian is the same, and evaluating the action interval from time t_1 to time t_2 gives

$$S = \int_{t_1}^{t_2} \mathcal{L}\, dt = \left[\frac{1}{2}mv_1^2 t - mv_1 g t^2 + \frac{1}{3}mg^2 t^3 - mgz_1 t\right]_{t_1}^{t_2}. \tag{A.7}$$

The positions and velocities at time t_1 in this expression are now different because of the π pulse. After the π pulse the atoms on the lower path received a momentum kick and acquired velocity v_0. As a result the position and velocity at t_1 along the lower path is

$$z_{lower1} = -\frac{1}{2}gt_1^2 \qquad \text{and} \tag{A.8a}$$

$$\dot{z}_{lower1} = v_0 - gt_1. \tag{A.8b}$$

Meanwhile the π pulse de-excits the atoms on the upper path, so the position and velocity of atoms on the upper path at time t_1 are

$$z_{upper1} = v_0 t_1 - \frac{1}{2} g t_1^2 \quad \text{and} \tag{A.9a}$$

$$\dot{z}_{upper1} = -g t_1. \tag{A.9b}$$

Plugging these values in for both paths from t_1 to t_2 and adding to the result for t_0 to t_1

$$\begin{aligned} S_{upper} = {} & \frac{1}{2} m v_0^2 t_1 - m g v_0 t_1^2 + \frac{1}{3} m g^2 t_1^3 + m g^2 t_1^2 (t_2 - t_1) + m g^2 t_1 (t_2 - t_1)^2 \\ & + \frac{1}{3} m g^2 (t_2 - t_1)^3 - m g v_0 t_1 (t_2 - t_1) \quad \text{and} \end{aligned} \tag{A.10a}$$

$$\begin{aligned} S_{lower} = {} & \frac{1}{3} m g^2 t_1^3 + \frac{1}{2} m v_0^2 (t_2 - t_1) + m g^2 t_1^2 (t_2 - t_1) - m g v_0 t_1 (t_2 - t_1) \\ & - m g v_o (t_2 - t_1)^2 + m g^2 t_1 (t_2 - t_1)^2 + \frac{1}{3} m g^2 (t_2 - t_1)^3. \end{aligned} \tag{A.10b}$$

Taking $S_{upper} - S_{lower}$ gives

$$S_{upper} - S_{lower} = \frac{1}{2} m v_0^2 t_1 - m g v_0 t_1^2 - \frac{1}{2} m v_0^2 (t_2 - t_1) + m g v_0 t_1 (t_2 - t_1). \tag{A.11}$$

Additionally, the final position of atoms along the upper and lower paths is

$$z_{upper2} = v_0 t_1 - \frac{1}{2} g t_1^2 - g t_1 (t_2 - t_1) - \frac{1}{2} g (t_2 - t_1)^2 \quad \text{and} \tag{A.12}$$

$$z_{lower2} = -\frac{1}{2} g t_1^2 + (v_0 - g t_1)(t_2 - t_1) - \frac{1}{2} g (t_2 - t_1)^2. \tag{A.13}$$

Up to this point I have not placed any constraints on the timing between the pulses of light. In order to have equal intervals between the $\pi/2$, π, and $\pi/2$ pulses, I let t_2=2t_1. This ensures that the interferometer closes in both position and momentum, which is a necessary condition to have an interferometer. As a result t_2-t_1 becomes t_1, which I let equal T. Therefore the equation for $S_{upper} - S_{lower}$ is

$$S_{upper} - S_{lower} = \frac{1}{2} m v_0^2 T - m g v_0 T^2 - \frac{1}{2} m v_0^2 T + m g v_0 T^2. \tag{A.14}$$

Evaluating this expression, difference between the upper and lower paths is

$$S_{upper} - S_{lower} = 0. \tag{A.15}$$

Additionally, with equal time intervals the final positions are

$$z_{upper2} = v_0 T - \frac{1}{2} g T^2 - g T^2 - \frac{1}{2} g T^2 \quad \text{and} \tag{A.16}$$

$$z_{lower2} = -\frac{1}{2} g T^2 + v_0 T - g T^2 - \frac{1}{2} g T^2. \tag{A.17}$$

Simplifying these expressions shows that they are equal and that an atom ends up in the same position whether it goes on the upper or lower path. The position of the atoms at the time of the final $\frac{\pi}{2}$ pulse is

$$z_2 = v_0 T - 2 g T^2. \tag{A.18}$$

These results shows that if the time between light pulses is equal, there is no difference in phase between the upper or the lower paths from classical effects. This is expected from a classical perspective since the atoms spend equal time with and without the momentum kick and end up in the same place at the same time. If classical phase was the only effect present, all of the atoms would be in the ground state after the final $\pi/2$ pulse and there is not a true interferometer. In the above analysis, I did not consider any phase effect from the laser pulses that transfer the atoms between the ground and excited states. When the light interacts with the atoms it imprints its phase on the atoms, and the accumulation of this phase explains the output of an atom interferometer. In order to quantify these effects I will start with the probability amplitude for the excited and ground state of a two level system, which given in [4] as a function of time are

$$c_e = c_{e0} cos(\frac{\Omega t}{2}) - i c_{go} e^{-i\phi} sin(\frac{\Omega t}{2}) \quad \text{and} \tag{A.19a}$$

$$c_g = -i c_{e0} e^{i\phi} sin(\frac{\Omega t}{2}) + c_{go} cos(\frac{\Omega t}{2}), \tag{A.19b}$$

where Ω is the Rabi frequency and ϕ is the phase of the laser light when it interacts with the population of atoms. For the π and $\frac{\pi}{2}$ pulses the quantity Ωt will equal π and $\frac{\pi}{2}$ respectively.

Since all atoms are initially in the ground state c_{e0} is 0 and c_{g0} is 1. After the first $\frac{\pi}{2}$ pulse the probability amplitudes are

$$c_{e1} = \frac{-i}{\sqrt{2}} e^{i\phi_0} \qquad \text{and} \tag{A.20a}$$

$$c_{g1} = \frac{-i}{\sqrt{2}}. \tag{A.20b}$$

Using these results as the initial probability amplitudes and re-evaluating Equations A.19a and A.19b, the probability amplitudes after the π pulse are

$$c_{e2} = \frac{-i}{\sqrt{2}} e^{-i\phi_{1L}} \qquad \text{and} \tag{A.21a}$$

$$c_{g2} = \frac{-1}{\sqrt{2}} e^{i(\phi_{1U}-\phi_0)}. \tag{A.21b}$$

Repeating the process for the second $\frac{\pi}{2}$ pulse, the final excited state probability amplitude is

$$c_{ef} = \frac{-i}{2} e^{-i\phi_{1L}} - \frac{i}{2} e^{i(-\phi_0+\phi_{1U}-\phi_2)}. \tag{A.22}$$

Taking the modulus squared to find the probability of finding an atom in the excited state after going through the interferometer gives

$$|c_{ef}|^2 = (\frac{i}{2} e^{i\phi_{1L}} + \frac{i}{2} e^{-i(-\phi_0+\phi_{1U}-\phi_2)})(\frac{-i}{2} e^{-i\phi_{1L}} - \frac{i}{2} e^{i(-\phi_0+\phi_{1U}-\phi_2)}). \tag{A.23}$$

Mutliplying this expression out and simplifying gives

$$|c_{ef}|^2 = \frac{1}{2} - e^{i(\phi_{1L}-\phi_0+\phi_{1U}-\phi_{2U})} - e^{-i(\phi_{1L}-\phi_0+\phi_{1U}-\phi_2)}. \tag{A.24}$$

The next step is to determine the total phase difference by evaluating the exponential. Each of the phase terms represents the phase of the laser light when it interacts with the atoms as

they move through the interferometer. As a result the phase for each point is the wavenumber of the laser times the position of that atoms at that time. Since the wavenumber of the laser light is the same for both all pulses of light the expression for phase becomes

$$\phi_{1L} - \phi_0 + \phi_{1U} - \phi_2 = k(z_{lower1} - z_0 + z_{upper1} - z_2). \tag{A.25}$$

Plugging in the appropriate positions from (A.8), (A.9), and (A.18) the total phase difference is

$$\Delta\phi = \phi_{1L} - \phi_0 + \phi_{1U} - \phi_2 = kgT^2. \tag{A.26}$$

Using this result in (A.24), and applying the definition of cosine, the probability that an atom will be in the excited state after going through the interferometer is

$$|c_{ef}|^2 = \frac{1}{2}(1 - cos(\Delta\phi)) \tag{A.27}$$

where $\Delta\phi = kgT^2$.

Overall this calculation shows a phase difference between the two paths of the atom interferometer due to the phase of the laser light that excites and de-excites the atoms. The classical action along the two paths is the same provided the time between pulses is the same. However in this interpretation, the laser light imprints its phase on the atoms and enables the precision measurements of atom interferometry.

A.2 Interferometer Phase via Quantum Mechanics

In this section, I derive the output of the atom interferometer by considering how the laser pulses in the interferometer impact the Hamiltonian of the system. Starting with the initial state of the atoms, I assume that all atoms are initially in the ground state. Therefore the initial wavefunction of the system can be written as

$$|\psi_o\rangle = \begin{pmatrix} 0 \\ 1 \end{pmatrix}. \tag{A.28}$$

Next in the interferometer sequence is the $\pi/2$ pulse which functions as a beam splitter. I define this as the operator, $\hat{S}$, given by

$$\hat{S} = \frac{1}{\sqrt{2}}\begin{pmatrix} 1 & -i \\ -i & 1 \end{pmatrix}. \tag{A.29}$$

After the beams are split they propagate in time according to the time evolution operator for their respective state. For the excited state and ground states these are

$$\hat{U}_e = e^{\frac{i}{\hbar}\hat{H}_e T} \qquad \text{and} \tag{A.30a}$$

$$\hat{U}_g = e^{\frac{i}{\hbar}\hat{H}_g T}. \tag{A.30b}$$

In these equations $\hat{H}_e$ and $\hat{H}_g$ represent the Hamiltonian's of the respective state given by

$$\hat{H}_e = \frac{(\hat{p} + \hbar k)^2}{2m} + mg\hat{z} \qquad \text{and} \tag{A.31a}$$

$$\hat{H}_g = \frac{\hat{p}^2}{2m} + mg\hat{z}. \tag{A.31b}$$

The difference between the two Hamiltonians is the additional momentum, expressed as $\hbar$k, supplied by the laser pulse. Putting this together, the total propagation operator is

$$\hat{P} = \begin{pmatrix} \hat{U}_e & 0 \\ 0 & \hat{U}_g \end{pmatrix}. \tag{A.32}$$

The final operator represents the π pulse, which I define as:

$$\hat{M} = \begin{pmatrix} 0 & -i \\ -i & 0 \end{pmatrix}. \tag{A.33}$$

Using these operators, the equation for the entire interferometer is

$$|\psi_f\rangle = \hat{S}\hat{P}\hat{M}\hat{P}\hat{S}\,|\psi_o\rangle\,. \tag{A.34}$$

Plugging in the definitions for each of the operators gives

$$|\psi_f\rangle = \frac{1}{\sqrt{2}}\begin{pmatrix}1 & -i\\ -i & 1\end{pmatrix}\begin{pmatrix}\hat{U}_e & 0\\ 0 & \hat{U}_g\end{pmatrix}\begin{pmatrix}0 & -i\\ -i & 0\end{pmatrix}\begin{pmatrix}\hat{U}_e & 0\\ 0 & \hat{U}_g\end{pmatrix}\frac{1}{\sqrt{2}}\begin{pmatrix}1 & -i\\ -i & 1\end{pmatrix}|\psi_o\rangle\,. \tag{A.35}$$

Performing the matrix operations the final state is

$$|\psi_f\rangle = \frac{1}{2}\begin{pmatrix}-\hat{U}_e\hat{U}_g - \hat{U}_g\hat{U}_e & -i\hat{U}_e\hat{U}_g + i\hat{U}_g\hat{U}_e\\ i\hat{U}_e\hat{U}_g - i\hat{U}_g\hat{U}_e & -\hat{U}_e\hat{U}_g - \hat{U}_g\hat{U}_e\end{pmatrix}|\psi_o\rangle\,. \tag{A.36}$$

The parameter of interest is the population of atoms in the excited state at the output of the interferometer. The projection of the final state onto the excited state is

$$\langle e\,|\psi_f\rangle = \begin{pmatrix}1 & 0\end{pmatrix}\frac{1}{2}\begin{pmatrix}-\hat{U}_e\hat{U}_g - \hat{U}_g\hat{U}_e & -i\hat{U}_e\hat{U}_g + i\hat{U}_g\hat{U}_e\\ i\hat{U}_e\hat{U}_g - i\hat{U}_g\hat{U}_e & -\hat{U}_e\hat{U}_g - \hat{U}_g\hat{U}_e\end{pmatrix}\begin{pmatrix}0\\ 1\end{pmatrix}. \tag{A.37}$$

Performing the matrix operations gives

$$\langle e\,|\psi_f\rangle = \frac{i}{2}\langle\hat{U}_g\hat{U}_e - \hat{U}_e\hat{U}_g\rangle. \tag{A.38}$$

For notation purposes I include the $\langle\rangle$ brackets around the unitary operators to denote that I have taken the inner product of the quantum states. The next step is to evaluate the product of these unitary operators. This is not a straightforward multiplication of exponentials because the exponent terms contain operators. As a result I apply the Baker-Campbell-Hausdorff formula [22]:

$$e^{\hat{A}}e^{\hat{B}} = e^{\hat{A}+\hat{B}+\frac{1}{2}[\hat{A},\hat{B}]+\frac{1}{12}[\hat{A},[\hat{A},\hat{B}]]+\frac{1}{12}[\hat{B},[\hat{B},\hat{A}]]\ldots}. \tag{A.39}$$

At this point it is important to note that the commutators of the excited state Hamiltonian and the ground state Hamiltonian do not commute. The commutators of these two operators

are

$$\left[\hat{H}_g, \hat{H}_e\right] = i\hbar^2 kg \qquad \text{and} \tag{A.40a}$$

$$\left[\hat{H}_e, \hat{H}_g\right] = -i\hbar^2 kg. \tag{A.40b}$$

Since both of these commutators are scalars, they both commute with the excited and ground state Hamiltonians. As a result the higher order terms of the Baker-Campbell-Hausdorff formula are zero and only first three terms of the exponent contribute. Applying the Baker-Campbell-Hausdorff formula with the commutators to (A.38) gives

$$\langle e\,|\psi_f\rangle = \frac{i}{2}\langle e^{\frac{i(\hat{H}_g+\hat{H}_e)T}{\hbar}-\frac{ikgT^2}{2}} - e^{\frac{i(\hat{H}_e+\hat{H}_g)T}{\hbar}+\frac{ikgT^2}{2}}\rangle. \tag{A.41}$$

To find the probability that a given atom is be in the excited state I take the modulus squared of the projection on the excited state:

$$\begin{aligned} |\langle e\,|\psi_f\rangle|^2 = {} & \frac{-i}{2}(e^{\frac{-i(\hat{H}_g+\hat{H}_e)T}{\hbar}+\frac{ikgT^2}{2}} - e^{\frac{-i(\hat{H}_e+\hat{H}_g)T}{\hbar}-\frac{ikgT^2}{2}}) \\ & \frac{i}{2}(e^{\frac{i(\hat{H}_g+\hat{H}_e)T}{\hbar}-\frac{ikgT^2}{2}} - e^{\frac{i(\hat{H}_e+\hat{H}_g)T}{\hbar}+\frac{ikgT^2}{2}}). \end{aligned} \tag{A.42}$$

When evaluating this product it is important to note that the sum of two operators is itself a new operator and every operator will commute with itself. As a result when I apply the Baker-Campbell-Hausdorff formula only the first terms in the exponent are nonzero. Therefore, the probability that the atom is in the excited state is

$$|\langle e\,|\psi_f\rangle|^2 = \frac{1}{4}(2 - e^{ikgT^2} - e^{-ikgT^2}). \tag{A.43}$$

Letting $\Delta\phi$=kgT^2, applying the definition of cosine, and simplifying the probability of finding an atom in the excited state after going through the interferometer becomes

$$|\langle e\,|\psi_f\rangle|^2 = \frac{1}{2}(1 - cos(\Delta\phi)). \tag{A.44}$$

Since the Hamiltonians for the excited state and the ground state do not commute, the two paths are not the same even though they reach the same point in space at the same time. If the Hamiltonians did commute the probability of the atom being in the excited state after the final pulse would be zero. In Appendix A.1, I found the phase difference between the paths by considering the classical action and phase of the laser light imprinted on the atom. Here, without any explicit use of laser phase, I found the same result coming from the non-commutivity of the ground and excited state Hamiltonians.

A.3 Interferometer Phase via Momentum Correction

In this section, I again derive the expression for the probability an atom is in the excited state after travelling through the interferometer, but I use a different definition of the Hamiltonian. In the previous section I defined the Hamiltonian as

$$\hat{H} = \frac{\hat{p}^2}{2m} + mg\hat{z}. \tag{A.45}$$

This is essentially the sum of kinetic and potential energy, specifically gravitational potential energy. For this calculation, I treat gravity differently. Instead of a potential energy I consider gravity to be a time dependent correction to the momentum of the atom. As a result, the expression for the excited and ground state Hamiltonians are:

$$\hat{H}_e = \frac{(\hat{p} + \hbar k + mgt)^2}{2m} \qquad \text{and} \tag{A.46a}$$

$$\hat{H}_g = \frac{(\hat{p} + mgt)^2}{2m}. \tag{A.46b}$$

Since the Hamiltonian is no longer constant in time, the time evolution operator over an arbitrary time interval, t_1 to t_2, is

$$\hat{U} = e^{\frac{i}{\hbar}\int_{t_1}^{t_2} \hat{H} dt}, \tag{A.47}$$

where $\hat{H}$ is either the ground or excited state Hamiltonian depending on the state of the atom over the time interval. In order to construct the time evolution operator for a specific interval it is necessary to define the corresponding limits of integration. With an equal interval between the $\pi/2$, π, and $\pi/2$ pulses, the limits of integration for the period between

the $\pi/2$ and π pulse is 0 to T, and the limits of integration for the period between the π and $\pi/2$ pulse are T to $2T$.

Considering first the lower path of the interferometer the operator $\hat{G}_1$ represents an atom in the ground state between the initial $\pi/2$ pulse and π pulse and the operator $\hat{E}_2$ that represents an atom in the excited state between the π pulse and final $\pi/2$ pulse:

$$\hat{G}_1 = \int_0^T \frac{(\hat{p} + mgt)^2}{2m} dt \qquad \text{and} \tag{A.48a}$$

$$\hat{E}_2 = \int_T^{2T} \frac{(\hat{p} + \hbar k + mgt)^2}{2m} dt. \tag{A.48b}$$

For the upper path, $\hat{E}_1$ represents an atom in the excited state between the initial $\pi/2$ pulse and π pulse, and $\hat{G}_2$, describes an atom in the ground state between the π pulse and final $\pi/2$ pulse:

$$\hat{E}_1 = \int_0^T \frac{(\hat{p} + \hbar k + mgt)^2}{2m} dt \qquad \text{and} \tag{A.48c}$$

$$\hat{G}_2 = \int_T^{2T} \frac{(\hat{p} + mgt)^2}{2m} dt. \tag{A.48d}$$

Evaluating the integrals with the appropriate limits for each of these operators gives

$$\hat{G}_1 = \frac{T}{2m}\hat{p}^2 + \frac{1}{2}gT^2\hat{p} + \frac{1}{6}mg^2T^3, \tag{A.49a}$$

$$\hat{E}_2 = \frac{T}{2m}\hat{p}^2 + \frac{\hbar kT}{m}\hat{p} + \frac{3}{2}gT^2\hat{p} + \frac{3}{2}\hbar kgT^2 + \frac{\hbar^2k^2}{2m} + \frac{7}{6}mg^2T^3, \tag{A.49b}$$

$$\hat{E}_1 = \frac{T}{2m}\hat{p}^2 + \frac{\hbar kT}{m}\hat{p} + \frac{1}{2}gT^2\hat{p} + \frac{1}{2}\hbar kgT^2 + \frac{\hbar^2k^2}{2m} + \frac{1}{6}mg^2T^3, \text{ and} \tag{A.49c}$$

$$\hat{G}_2 = \frac{T}{2m}\hat{p}^2 + \frac{3}{2}gT^2\hat{p} + \frac{7}{6}mg^2T^3. \tag{A.49d}$$

Since all other operators and conditions are the same as the previous section, the projection of the interferometer output onto the excited state remains as shown in (A.38):

$$\langle e\,|\psi_f\rangle = \frac{i}{2}\langle \hat{U}_g\hat{U}_e - \hat{U}_e\hat{U}_g\rangle. \tag{A.50}$$

As a reminder, the $\langle\rangle$ brackets around the unitary operators denote that I have taken the inner product of the quantum states. Substituting the appropriate operator for each segment of the interferometer, the equation becomes

$$\langle e\,|\psi_f\rangle = \frac{i}{2}\langle(\hat{U}_{G2}\hat{U}_{E1} - \hat{U}_{E2}\hat{U}_{G1})\rangle \qquad \text{and then} \tag{A.51}$$

$$\langle e\,|\psi_f\rangle = \frac{i}{2}\langle(e^{\frac{i}{\hbar}\hat{G}_2}e^{\frac{i}{\hbar}\hat{E}_1} - e^{\frac{i}{\hbar}\hat{E}_2}e^{\frac{i}{\hbar}\hat{G}_1})\rangle. \tag{A.52}$$

The next step in the calculation is to take the modulus squared to find the probability that an atom is in the excited state. Since $\hat{G}_1$, $\hat{G}_2$, $\hat{E}_1$ and $\hat{E}_2$ are all composed of either scalar numbers or various powers of the momentum operator, they commute in any combination, and only the first two terms are nonzero when I apply the Baker-Campbell-Hausdorff formula. Putting this together, the modulus squared is

$$|\langle e\,|\psi_f\rangle\,|^2 = \frac{1}{4}(2 - e^{\frac{i}{\hbar}(\hat{E}_2+\hat{G}_1-\hat{G}_2-\hat{E}_1)} - e^{\frac{-i}{\hbar}(\hat{E}_2+\hat{G}_1-\hat{G}_2-\hat{E}_1)}). \tag{A.53}$$

Using (A.49a) through (A.49d) the sum of the operators in the exponential is

$$\hat{E}_2 + \hat{G}_1 - \hat{G}_2 - \hat{E}_1 = \hbar k g T^2. \tag{A.54}$$

Plugging this result into the expression for the probability gives

$$|\langle e\,|\psi_f\rangle\,|^2 = \frac{1}{4}(2 - e^{ikgT^2} - e^{-ikgT^2}). \tag{A.55}$$

Just as in the previous sections, I let $\Delta\phi$=kgT^2 and apply the definition of cosine to find that the probability an atom is in the excited state after going through the interferometer is

$$|\langle e\,|\psi_f\rangle\,|^2 = \frac{1}{2}(1 - cos(\Delta\phi)). \tag{A.56}$$

This is the same result as in Appendix A.1 and A.2. In the previous section, the phase difference between the upper and lower paths of the interferometer came from the non-commutivity of the ground and excited state Hamiltonians. Here the phase difference

comes from the fact that the correction term to momentum increases with increasing time. As a result the correction factor applied to the $\hbar k$ term in the momentum is different for the upper and lower path of the interferometer. Since the upper path is in the excited state earlier than the lower path, its $\hbar k$ momentum addition is affected differently by the mgt term than the lower path which is in the excited state later. As a result there is a phase difference between the two paths.

THIS PAGE INTENTIONALLY LEFT BLANK

APPENDIX B:
Laser Locking Criteria

In this Appendix, I provide the criteria for determining if the optical system's frequency lock is effective. First, I introduce the concept of Allan deviation and how I use it to assess the frequency stability of a laser. Next I consider how error in the laser's frequency affects the number of atoms a MOT can capture and compare it to the effects of shot noise. Finally, I analyze how factors such as the strength of the coupling between the laser and the transition, jittering of the laser frequency, and the amount of detuning from resonance influence how well a laser drives a target transition.

B.1 Allan Deviation

An important parameter for evaluating the stability of a laser's frequency is Allan deviation (ADEV) [23], [24]. ADEV is calculated by averaging data over various time intervals, then finding the average difference between each interval. If the variation in a data set is dominated by random noise, the ADEV will decrease with increasing averaging time. When the variation is dominated by a fundamental drift of the data the ADEV will increase with increasing averaging time. On a logarithmic plot of ADEV vs time constants for a set of data, the minimum value of ADEV shows the averaging time at which the transition from averaging down to averaging up occurs. This time constant provides an estimate of the time scale over which the system is stable under the influence of drifts.

For an example to illustrate the utility of ADEV, I consider a simple model of random noise added to a linear drift. Figure B.1 shows examples of this signal with different drift slopes and noise levels.

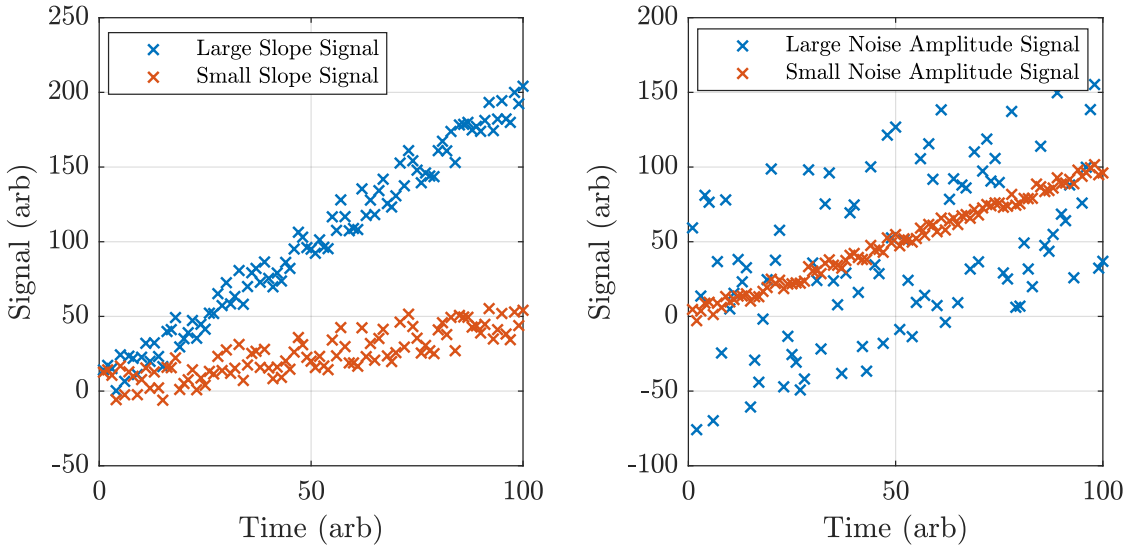

Figure B.1. Sample signals with different (a) drift slopes and (b) noise levels.

I calculated the ADEV of several signals like those shown in Figure B.1 using the built in MATLAB function `allanvar` and taking the square root. This function returns the Allan variance which is the square of the Allan deviation. Figure B.2a shows a plot of the ADEV vs averaging time for several of these signals with various drift slopes but constant noise amplitude. Figure B.2b shows ADEV vs averaging time for signals with a constant drift slope and various noise amplitudes.

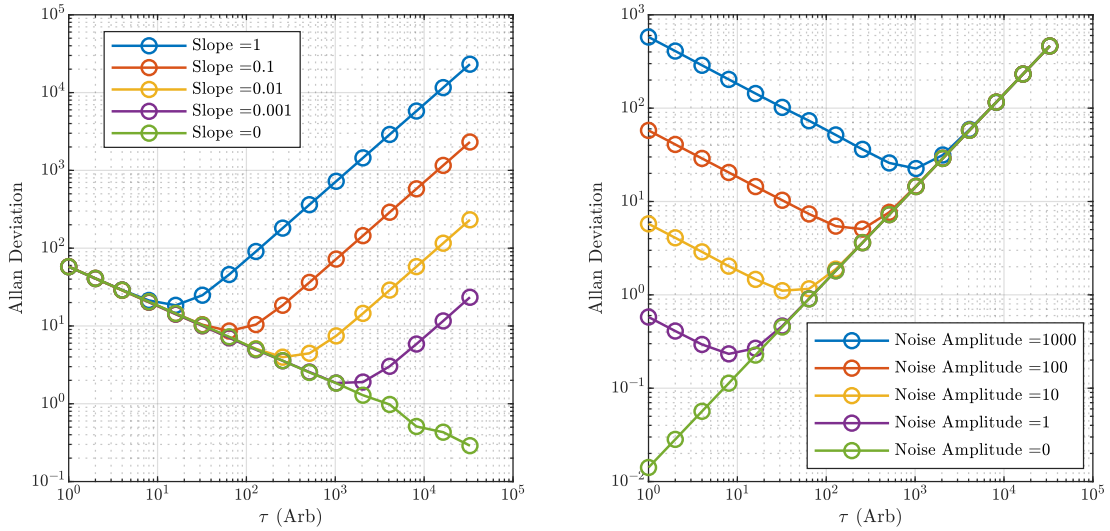

Figure B.2. Allan deviation for signals with various (a) drift slopes and (b) noise levels.

Figure B.2 shows that as the slope of the drift decreases the minimum value of ADEV decreases and occurs at greater averaging times. The reason is that at lower slopes, random noise dominates the variability of the signal and greater averaging reduces this noise and the variability. Said another way, a smaller underlying drift allows the opportunity to average away more noise before the impact of the drift becomes significant. The second trend is that as noise increases with a constant slope, the minimum ADEV increases and shifts to longer averaging time. This is because the higher random noise stays the dominant factor for longer before the drift takes over so the minimum occurs at a longer averaging time. The minimum ADEV also increases with greater noise because there is so much noise that it cannot be averaged down before the drift becomes significant.

It is particularly useful to examine the limiting cases when there is either no drift or no noise. When slope is 0, there is no drift and the only contribution to variation is random noise. This is why, as can be seen on the slope = 0 curve in Figure B.2, no matter how long the averaging time is the ADEV keeps decreasing. Conversely when there is no noise, increasing averaging time only increases the ADEV because there is no random noise to average away as shown on the zero noise amplitude curve of Figure B.2.

For laser stability, ADEV is a very important tool to evaluate the effectiveness of a locking system. Monitoring laser frequency over a time interval and then calculating the ADEV of that data characterizes the magnitude and timescales of frequency drifts and frequency noise. If the laser does not have a long term frequency drift ADEV would continuously decrease with increasing averaging time. Additionally if the laser frequency noise oscillations are small, the ADEV would quickly reach a minimum, but if there is no long term drift it will not immediately start to increase and will instead remain constant with increasing averaging time. Therefore the plot of ADEV vs averaging time for a laser with no drift and minimal noise would have a hockey stick shape. There will always be some level of noise in the frequency so this outcome is not practical, but an effective laser lock should have continued averaging down of deviation over the time period of interest.

Overall, the ADEV of laser frequency characterizes the effectiveness of the lock and helps determine the sources of frequency instability. The value of the ADEV as well as the shape of the curve when plotted versus averaging time illustrate whether drifts exist, the point they become significant, and the impact of noisy oscillations of the laser frequency.

B.2 Frequency Error and Shot Noise

In steady state, a two level system in the presence of a driving laser has a probability of being in the excited state given by

$$p_{22} = \frac{\Omega^2}{2\Omega^2 + 4\beta^2 + 4\delta^2} \tag{B.1}$$

where Ω is the Rabi frequency, β is one half the decay rate from the excited to the ground state, and δ is the detuning or difference between the laser frequency and the resonant frequency of the transition [25]. The units of all terms are radians per second. In order to determine how changes in the laser frequency affect this probability I take the derivative of this function with respect to detuning

$$\frac{\partial p_{22}}{\partial \delta} = \frac{-8\delta\Omega^2}{(2\Omega^2 + 4\beta^2 + 4\delta^2)^2}. \tag{B.2}$$

In order to find a normalized expression for the change in probability, I move $\partial\delta$ to the right side of (B.2) and divide both sides by (B.1). After simplifying, the results is

$$\frac{\partial p_{22}}{p_{22}} = \frac{-4\delta\partial\delta}{2\Omega^2 + 4\beta^2 + 4\delta^2}. \tag{B.3}$$

The change in the number of atoms in the MOT due to atom shot noise is $\frac{1}{\sqrt{N}}$ where N is the number of atoms in the MOT. Substituting this into (B.3) and rearranging to solve for $\partial\delta$ gives

$$\partial\delta = \frac{-1}{\sqrt{N}} \frac{\Omega^2 + 2\beta^2 + 2\delta^2}{4\delta}. \tag{B.4}$$

(B.4) estimates how large $\partial\delta$ can be before laser jitter rather than atomic statistics becomes the determining factor for how many atoms the MOT can consistently capture. Considering the blue cooling transition (461 nm) for the MOT I plug in values to (B.4) to estimate how stable our laser frequency needs to be. The 461 nm transition has a frequency of 32 MHz which gives a β of 32π MHz. In a MOT, a typical detuning, δ, is 2β. Additionally a typical Rabi frequency for a MOT is 10β. Using these values as well as $N = 1x10^6$, (B.4)

estimates that our laser must be locked to approximately 1.4 MHz. Trapping one million atoms would be serviceable for atom interferometry in the 30 meter tower, but to truly make highly precise measurements, the goal is to trap closer to 1 billion atoms. For this value of N, (B.4) estimates that the laser must be locked to approximately 44 kHz.

Locking a laser to an order of 44 kHz is a significant technical challenge. For the purpose of atom interferometry in the 30 meter tower, locking a laser to the order of kilohertz is not practical or a judicious use of resources. Realistically this estimate means that the number of atoms we can trap in the MOT will somewhat depend on jitter in laser frequency. Since the MOT is not be shot noise limited when trapping higher number of atoms,it is necessary to consider how well the laser frequency must be locked to effectively drive the atomic transitions that control the atoms in the experiment.

B.3 Laser Jitter and Performance

One important consideration in determining how well the laser must be locked is the ability to reliably drive the targeted electronic transition. The steady state probability that an atom will be in the excited state due to excitation from a laser with a finite linewidth is

$$p_{22} = \frac{\Omega^2(1+\frac{\lambda}{\beta})}{2\Omega^2(1+\frac{\lambda}{\beta})+4(\beta+\lambda)^2+4\delta^2}, \tag{B.5}$$

where λ represents the linewidth of the laser [26]. This equation describes how the coupling strength between the laser and the transition as well as the laser linewidth impact the laser's ability to drive the target transition. Starting with the strength of the coupling, Figure B.3 shows the excited state probability as a function of detuning for various ratios of Rabi frequency to transition linewidth using monochromatic light ($\lambda = 0$). The obvious trend is that as the Rabi frequency increases relative to the decay rate of the transition, the probability of being in the excited state increases. Notably at low couplings, $\Omega = .1\beta$, the probability of the atom being in the excited state is effectively zero.

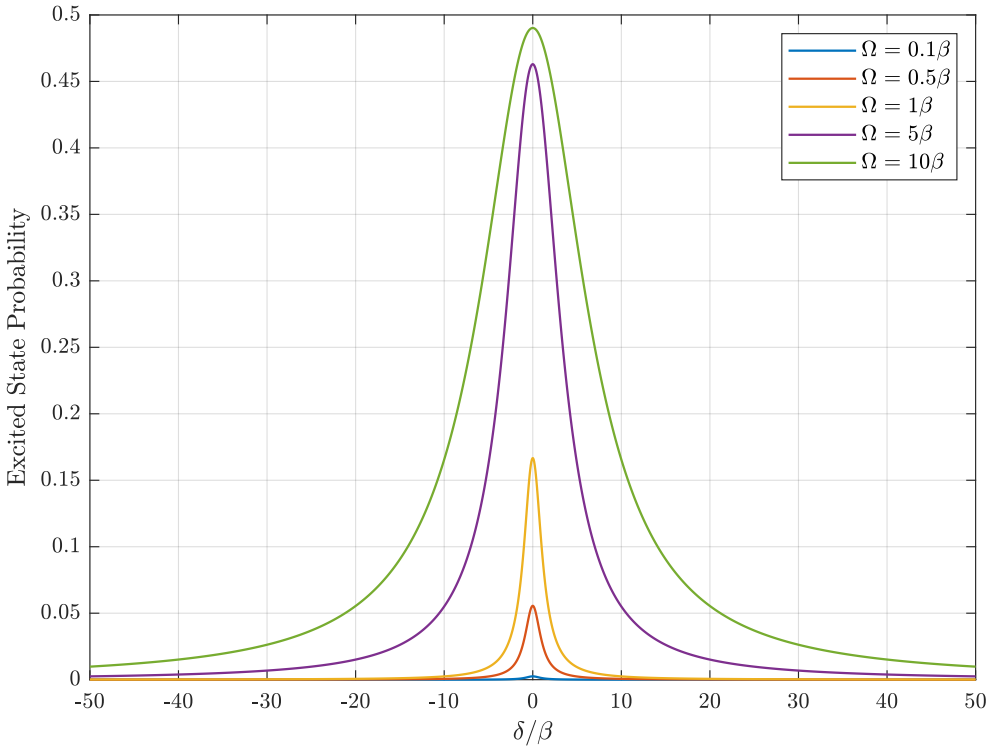

Figure B.3. Excited state probability vs. laser detuning for monochromatic light at various Rabi frequencies.

The next step is to examine the impact of the laser's linewidth. I consider that laser frequency jitter behaves like and has similar effects as the natural linewidth of the laser. This means that I use the linewidth of the laser to examine the effects of frequency's jitter. For this part of the analysis I set the Rabi frequency to a multiple of β and varied the linewidth of the laser. Figure B.4 plots the excited state probability as a function of detuning for various laser linewidths for a Rabi frequency of $\Omega = 5\beta$ and $\Omega = \beta$.

These plots also show several important differences between the strongly and weakly coupled case. First the excited state probability for all laser linewidths is significantly lower for the weakly coupled case for all values of detuning. Second, the excited state probability for a given detuning falls off quicker with increased linewidth for the weakly coupled case than the strongly coupled case. Additionally the excited state probability decreases faster from the peak value with increasing detuning in the weakly coupled case. These observations reinforce the point from above that the ability of a laser to drive a transition is highly dependent on the coupling strength.

The general trend is that as laser linewidth increases, the peak probability decreases and

the distribution gets wider. Additionally both plots show a significant drop in excited state probability between the $\lambda = \beta$ and $\lambda = 5\beta$ case. From this observation the conclusion is that if the range of the laser's jitter is much less than the linewidth of the transition, the laser system will be effective at driving it.

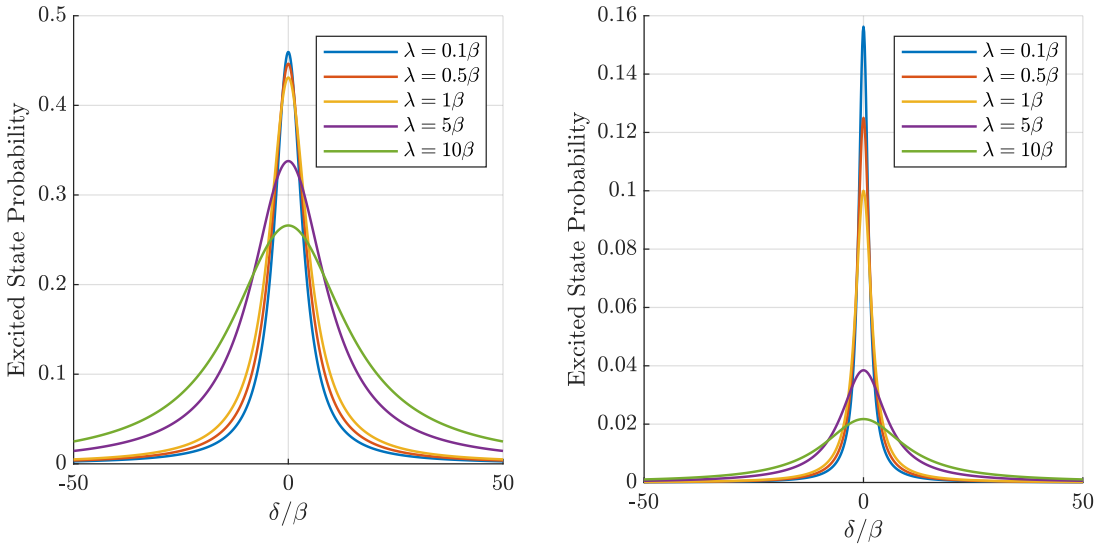

Figure B.4. Excited state probability vs. laser detuning at (a) $\Omega = 5\beta$ and (b) $\Omega = \beta$.

For developing a laser frequency locking system indicators like ADEV and limiting the jitter of the frequency are useful metrics. Overall an effective laser locking system minimizes drifts and keeps laser jitter less than the linewidth of the target transition while using the minimum amount of laser power so that most of the output can be sent to the experiment, maximizing coupling. Ultimately though, the indicator of an effective laser locking system is whether the lasers are stable enough to form a MOT.

THIS PAGE INTENTIONALLY LEFT BLANK

List of References

[1] A. Peters, K. Y. Chung, and S. Chu, "High-precision gravity measurements using atom interferometry," *Metrologia*, vol. 38, no. 1, pp. 25–61, 2001.

[2] A. Peters, K. Y. Chung, B. Young, J. Hensley, and S. Chu, "Precision atom interferometry," *Philosophical transactions of the Royal Society of London. Series A: Mathematical, physical, and engineering sciences*, vol. 355, no. 1733, pp. 2223–2233, 1997.

[3] T. Mazzoni, X. Zhang, R. Del Aguila, L. Salvi, N. Poli, and G. M. Tino, "Large-momentum-transfer bragg interferometer with strontium atoms," *Phys. Rev. A*, vol. 92, p. 053619, Nov. 2015. Available: https://link.aps.org/doi/10.1103/PhysRevA.92.053619

[4] J. Davis and F. Narducci, "A proposal for a gradient magnetometer atom interferometer," *Journal of Modern Optics*, vol. 55, no. 19-20, pp. 3173–3185, 2008. Available: https://doi.org/10.1080/09500340802468633

[5] T. Gustavson, P. Bouyer, and M. Kasevich, "Precision rotation measurements with an atom interferometer gyroscope," *Physical review letters*, vol. 78, no. 11, pp. 2046–2049, 1997.

[6] S. Abend, M. Gersemann, C. Schubert, D. Schlippert, E. Rasel, M. Zimmermann, M. Efremov, A. Roura, F. Narducci, and W. Schleich, "Atom interferometry and its applications," 2019. Available: https://calhoun.nps.edu/handle/10945/64996

[7] M. Zimmermann, M. A. Efremov, W. Zeller, W. P. Schleich, J. P. Davis, and F. A. Narducci, "Representation-free description of atom interferometers in time-dependent linear potentials," *New journal of physics*, vol. 21, no. 7, pp. 73 031–, 2019.

[8] P. D. Lett, W. D. Phillips, S. L. Rolston, C. E. Tanner, R. N. Watts, and C. I. Westbrook, "Optical molasses," *J. Opt. Soc. Am. B*, vol. 6, no. 11, pp. 2084–2107, Nov. 1989. Available: http://josab.osa.org/abstract.cfm?URI=josab-6-11-2084

[9] E. L. Raab, M. Prentiss, A. Cable, S. Chu, and D. E. Pritchard, "Trapping of neutral sodium atoms with radiation pressure," *Phys. Rev. Lett.*, vol. 59, pp. 2631–2634, Dec. 1987. Available: https://link.aps.org/doi/10.1103/PhysRevLett.59.2631

[10] M. Auzinsh, D. Budker, and S. Rochester, *Optically polarized atoms understanding light-atom interactions*. New York, USA: Oxford University Press, Incorporated, 2010. Available: https://ebookcentral.proquest.com/lib/ebook-nps/detail.action?docID=648031

[11] R. Dragoset, A. Musgrove, C. Clark, W. Martin, P. Mohr, C. Sturrock, and B. Taylor, "Periodic table: Atomic properties of the elements," [Online]. Available: http://physics.nist.gov/pt [2022, August 24], 1999.

[12] S. Stellmer, F. Schreck, and T. Kilian, "Degenerate quantum gases of strontium," in *Annual review of cold atoms and molecules, volume 2*, K. W. Madison, K. Bongs, C. L. D, K. Zhai, and A. M. Rey, Eds. Singapore: World Scientific Publishing Co. Pte. Ltd, 2014, pp. 1–80.

[13] A. Kramida, Yu. Ralchenko, J. Reader, and NIST ASD Team, NIST Atomic Spectra Database (ver. 5.9), [Online]. Available: https://physics.nist.gov/asd [2022, July 8]. National Institute of Standards and Technology, Gaithersburg, MD, USA, 2021.

[14] X. Xu, T. H. Loftus, J. L. Hall, A. Gallagher, and J. Ye, "Cooling and trapping of atomic strontium," *Journal of the Optical Society of America. B, Optical physics*, vol. 20, no. 5, pp. 968–, 2003.

[15] M. Boyd, "High precision spectroscopy of strontium in an optical lattice: Towards a new standard for frequency and time," Ph.D. dissertation, Department of Physics., University of Colorado, Boulder, CO, USA, 2007.

[16] I. Courtillot, A. Quessada-Vial, A. Brusch, D. Kolker, G. D. Rovera, and P. Lemonde, "Accurate spectroscopy of Sr atoms," *The European Physical Journal D : Atomic, Molecular, Optical and Plasma Physics*, vol. 33, p. 161, 2005, 12 pages, 16 figures. Available: https://hal.archives-ouvertes.fr/hal-00016398

[17] M. A. Norcia and J. K. Thompson, "Simple laser stabilization to the strontium 88sr transition at 707 nm," *Review of scientific instruments*, vol. 87, no. 2, pp. 023 110–023 110, 2016.

[18] S. Hartmann, J. Jenewein, E. Giese, S. Abend, A. Roura, E. M. Rasel, and W. P. Schleich, "Regimes of atomic diffraction: Raman versus bragg diffraction in retroreflective geometries," *Physical Review. A*, vol. 101, no. 5, 2020.

[19] *Wavelength Meter WS8-30 User Manual*, HighFinesse Laser and Electronic Systems, Tübingen, Germany, 2016.

[20] Y. Hayakawa, T. Sato, C. Watanabe, T. Aoki, and Y. Torii, "Doppler-free spectroscopy of metastable sr atoms using a hollow cathode lamp," *Applied Optics (2004)*, vol. 57, no. 6, pp. 1450–1454, 2018.

[21] *User Manual Stable 32: Frequency Stability Analysis*, Hamilton Technical Services, Beaufort, SC, USA, 2007.

[22] J. C. Moodie and M. W. Long, "An exact power series representation of the Baker-Campbell-Hausdorff formula," *Journal of Physics A: Mathematical and Theoretical*, vol. 54, no. 1, pp. 15 208–, 2020.

[23] F. Walls and D. Allan, "Measurements of frequency stability," *Proceedings of the IEEE*, vol. 74, no. 1, pp. 162–168, 1986.

[24] D. Allan, "Time and frequency (time-domain) characterization, estimation, and prediction of precision clocks and oscillators," *IEEE Transactions on Ultrasonics, Ferroelectrics, and Frequency Control*, vol. 34, no. 6, pp. 647–654, 1987.

[25] H. J. Kimble and L. Mandel, "Theory of resonance fluorescence," *Physical Review A.*, vol. 13, no. 6, pp. 2123–2144, 1976.

[26] H. J. Kimble and L. Mandel, "Resonance fluorescence with excitation of finite bandwidth," *Physical Review. A*, vol. 15, no. 2, pp. 689–699, 1977.

THIS PAGE INTENTIONALLY LEFT BLANK

Initial Distribution List

1. Defense Technical Information Center
   Ft. Belvoir, Virginia

2. Dudley Knox Library
   Naval Postgraduate School
   Monterey, California